Aerodynamics and fluid-structure interaction simulation with AMROC Part I

Ralf Deiterding

Aerodynamics and Flight Mechanics Research Group
University of Southampton
Highfield Campus
Southampton SO17 1BJ, UK
Email: r.deiterding@soton.ac.uk

Xiamen
24th July, 2019

Outline

Collaboration with

Finite volume methods

- Jose M. Garro Fernandez (University of Southampton)
- Stuart Laurence (Department of Aerospace Engineering, University of Maryland, College Park)
- Fehmi Cirak (Cambridge University)
- Sean Mauch, Joe Shepherd, Dan Meiron (California Institute of Technology)

Lattice Boltzmann methods

- Christos Gkoudesnes, Juan Antonio Reyes Barraza (University of Southampton)
- Stephen Wood (NASA)
- Kai Feldhusen, Claus Wagner (German Aerospace Center – DLR)
- Moritz Fragner (University of Applied Sciences Hannover, Germany)
- Cinar Laloglu (Marmara University, Turkey)

Construction of coupling data

- Moving boundary/interface is treated as a moving contact discontinuity and represented by level set [Fedkiw, 2002][Arienti et al., 2003]
- Efficient construction of level set from triangulated surface data with closest-point-transform (CPT) algorithm [Mauch, 2003]

Construction of coupling data

- Moving boundary/interface is treated as a moving contact discontinuity and represented by level set [Fedkiw, 2002][Arienti et al., 2003]
- Efficient construction of level set from triangulated surface data with closest-point-transform (CPT) algorithm [Mauch, 2003]
- One-sided construction of mirrored ghost cell and new FEM nodal point values

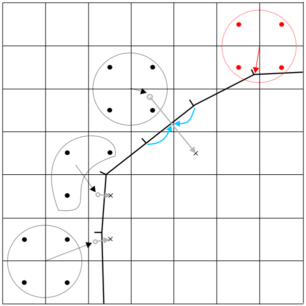

Construction of coupling data

- Moving boundary/interface is treated as a moving contact discontinuity and represented by level set [Fedkiw, 2002][Arienti et al., 2003]
- Efficient construction of level set from triangulated surface data with closest-point-transform (CPT) algorithm [Mauch, 2003]
- One-sided construction of mirrored ghost cell and new FEM nodal point values
- FEM ansatz-function interpolation to obtain intermediate surface values

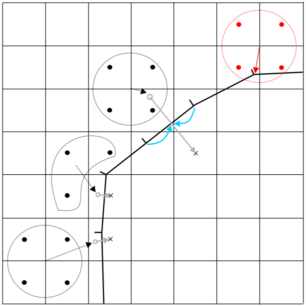

Coupling conditions on interface
Viscous fluid:

$$\left.\begin{array}{rcl} u^S & = & u^F \\ \sigma^S_{nm} & = & \sigma^F_{nm} \end{array}\right|_{\mathcal{I}}$$

with $\sigma^F_{nm} = -p^F \delta_{nm} + \Sigma^F_{nm}$

Construction of coupling data

- Moving boundary/interface is treated as a moving contact discontinuity and represented by level set [Fedkiw, 2002][Arienti et al., 2003]
- Efficient construction of level set from triangulated surface data with closest-point-transform (CPT) algorithm [Mauch, 2003]
- One-sided construction of mirrored ghost cell and new FEM nodal point values
- FEM ansatz-function interpolation to obtain intermediate surface values
- Explicit coupling possible if geometry and velocities are prescribed for the more compressible medium [Specht, 2000]

$$u^F := u^S(t)|_{\mathcal{I}}$$
$$\texttt{UpdateFluid(}\,\Delta t\,\texttt{)}$$
$$\sigma^S_{nm} := \sigma^F_{nm}(t+\Delta t)|_{\mathcal{I}}$$
$$\texttt{UpdateSolid(}\,\Delta t\,\texttt{)}$$
$$t := t + \Delta t$$

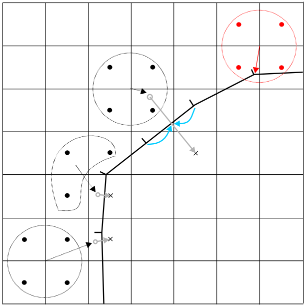

Coupling conditions on interface
Viscous fluid:

$$\left.\begin{array}{rcl} u^S & = & u^F \\ \sigma^S_{nm} & = & \sigma^F_{nm} \end{array}\right|_{\mathcal{I}}$$

with $\sigma^F_{nm} = -p^F \delta_{nm} + \Sigma^F_{nm}$

Construction of coupling data

- Moving boundary/interface is treated as a moving contact discontinuity and represented by level set [Fedkiw, 2002][Arienti et al., 2003]

- Efficient construction of level set from triangulated surface data with closest-point-transform (CPT) algorithm [Mauch, 2003]
- One-sided construction of mirrored ghost cell and new FEM nodal point values
- FEM ansatz-function interpolation to obtain intermediate surface values
- Explicit coupling possible if geometry and velocities are prescribed for the more compressible medium [Specht, 2000]

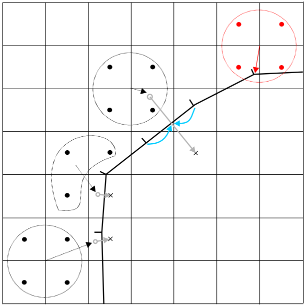

$$u_n^F := u_n^S(t)|_{\mathcal{I}}$$
`UpdateFluid(` Δt `)`
$$\sigma_{nm}^S := -p^F(t+\Delta t)\delta_{nm}|_{\mathcal{I}}$$
`UpdateSolid(` Δt `)`
$$t := t + \Delta t$$

Coupling conditions on interface
Inviscid fluid:

$$\left.\begin{aligned} u_n^S &= u_n^F \\ \sigma_{nm}^S &= -p^F\delta_{nm} \end{aligned}\right|_{\mathcal{I}}$$

Construction of coupling data

- Moving boundary/interface is treated as a moving contact discontinuity and represented by level set [Fedkiw, 2002][Arienti et al., 2003]

- Efficient construction of level set from triangulated surface data with closest-point-transform (CPT) algorithm [Mauch, 2003]
- One-sided construction of mirrored ghost cell and new FEM nodal point values
- FEM ansatz-function interpolation to obtain intermediate surface values
- Explicit coupling possible if geometry and velocities are prescribed for the more compressible medium [Specht, 2000]

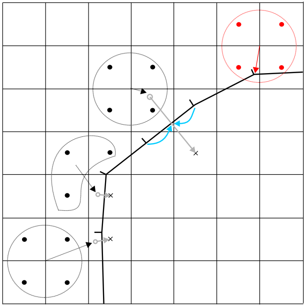

$$u_n^F := u_n^S(t)|_{\mathcal{I}} \qquad \sigma_{nm}^S := -p^F(t)\delta_{nm}|_{\mathcal{I}}$$
$$\texttt{UpdateFluid(}\,\Delta t\,\texttt{)} \qquad \texttt{UpdateSolid(}\,\Delta t\,\texttt{)}$$
$$t := t + \Delta t$$

[Deiterding and Wood, 2013]

Coupling conditions on interface
Inviscid fluid:

$$\left.\begin{array}{rcl} u_n^S & = & u_n^F \\ \sigma_{nm}^S & = & -p^F\delta_{nm} \end{array}\right|_{\mathcal{I}}$$

Closest point transform algorithm

The signed distance φ to a surface $\mathcal{I}$ satisfies the eikonal equation [Sethian, 1999]

$$|\nabla\varphi| = 1 \quad \text{with} \quad \varphi\big|_{\mathcal{I}} = 0$$

Solution smooth but non-diferentiable across characteristics.

Closest point transform algorithm

The signed distance φ to a surface $\mathcal{I}$ satisfies the eikonal equation [Sethian, 1999]

$$|\nabla\varphi| = 1 \quad \text{with} \quad \varphi\big|_{\mathcal{I}} = 0$$

Solution smooth but non-diferentiable across characteristics.

Distance computation trivial for non-overlapping elementary shapes but difficult to do efficiently for triangulated surface meshes:

- Geometric solution approach with plosest-point-transform algorithm [Mauch, 2003]

Closest point transform algorithm

The signed distance φ to a surface $\mathcal{I}$ satisfies the eikonal equation [Sethian, 1999]

$$|\nabla\varphi| = 1 \quad \text{with} \quad \varphi\big|_{\mathcal{I}} = 0$$

Solution smooth but non-diferentiable across characteristics.

Distance computation trivial for non-overlapping elementary shapes but difficult to do efficiently for triangulated surface meshes:

- Geometric solution approach with plosest-point-transform algorithm [Mauch, 2003]

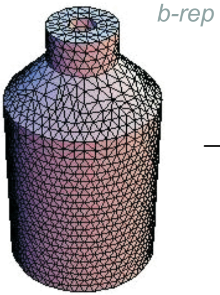

Surface mesh $\mathcal{I}$

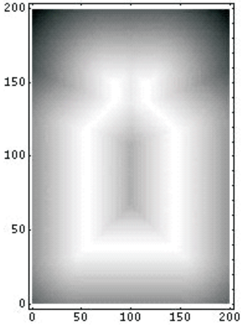

Distance φ

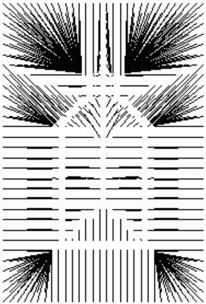

Normal to closest point

The characteristic / scan conversion algorithm

1. Build the characteristic polyhedrons for the surface mesh

Characteristic polyhedra for faces, edges, and vertices

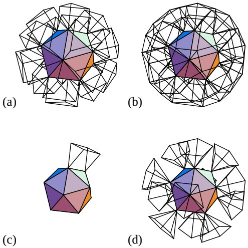

The characteristic / scan conversion algorithm

1. Build the characteristic polyhedrons for the surface mesh
2. For each face/edge/vertex
   2.1 Scan convert the polyhedron.

Characteristic polyhedra for faces, edges, and vertices

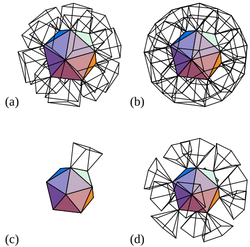

Slicing and scan conversion of apolygon

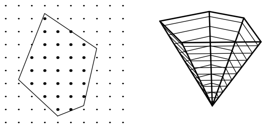

The characteristic / scan conversion algorithm

1. Build the characteristic polyhedrons for the surface mesh
2. For each face/edge/vertex
   2.1 Scan convert the polyhedron.
   2.2 Compute distance to that primitive for the scan converted points

Characteristic polyhedra for faces, edges, and vertices

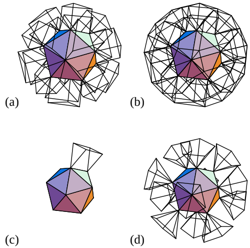

Slicing and scan conversion of apolygon

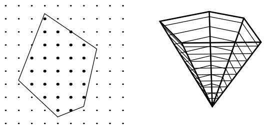

The characteristic / scan conversion algorithm

1. Build the characteristic polyhedrons for the surface mesh
2. For each face/edge/vertex
   2.1 Scan convert the polyhedron.
   2.2 Compute distance to that primitive for the scan converted points
3. Computational complexity.
   - $O(m)$ to build the b-rep and the polyhedra.
   - $O(n)$ to scan convert the polyhedra and compute the distance, etc.

Characteristic polyhedra for faces, edges, and vertices

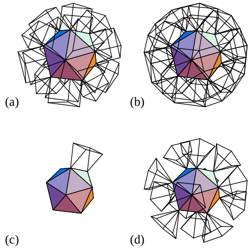

Slicing and scan conversion of apolygon

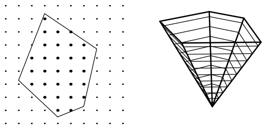

The characteristic / scan conversion algorithm

1. Build the characteristic polyhedrons for the surface mesh
2. For each face/edge/vertex
   2.1 Scan convert the polyhedron.
   2.2 Compute distance to that primitive for the scan converted points
3. Computational complexity.
   - $O(m)$ to build the b-rep and the polyhedra.
   - $O(n)$ to scan convert the polyhedra and compute the distance, etc.
4. Problem reduction by evaluation only within specified max. distance

[Mauch, 2003], see also [Deiterding et al., 2006]

Characteristic polyhedra for faces, edges, and vertices

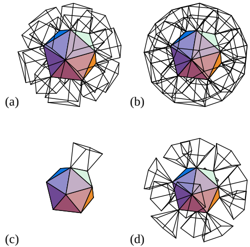

Slicing and scan conversion of apolygon

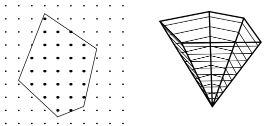

Eulerian/Lagrangian communication module

1. Put bounding boxes around each solid processors piece of the boundary and around each fluid processors grid

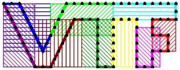

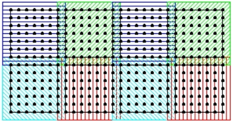

Eulerian/Lagrangian communication module

1. Put bounding boxes around each solid processors piece of the boundary and around each fluid processors grid
2. Gather, exchange and broadcast of bounding box information

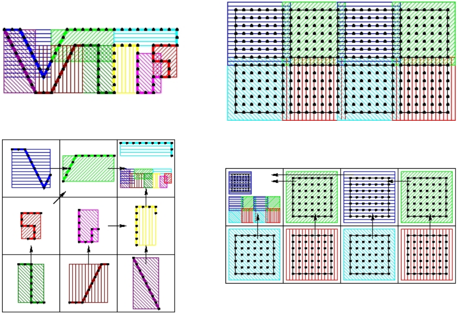

Eulerian/Lagrangian communication module

1. Put bounding boxes around each solid processors piece of the boundary and around each fluid processors grid
2. Gather, exchange and broadcast of bounding box information
3. Optimal point-to-point communication pattern, non-blocking

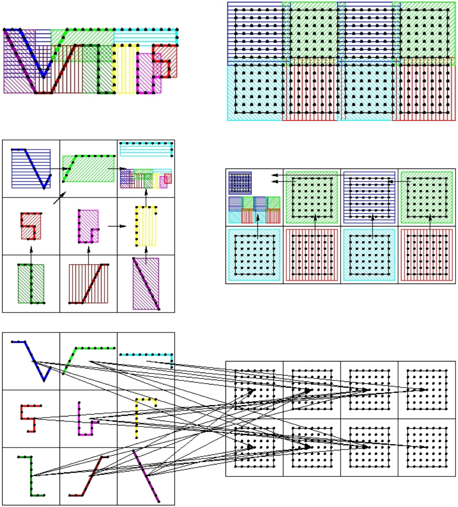

Coupling elements

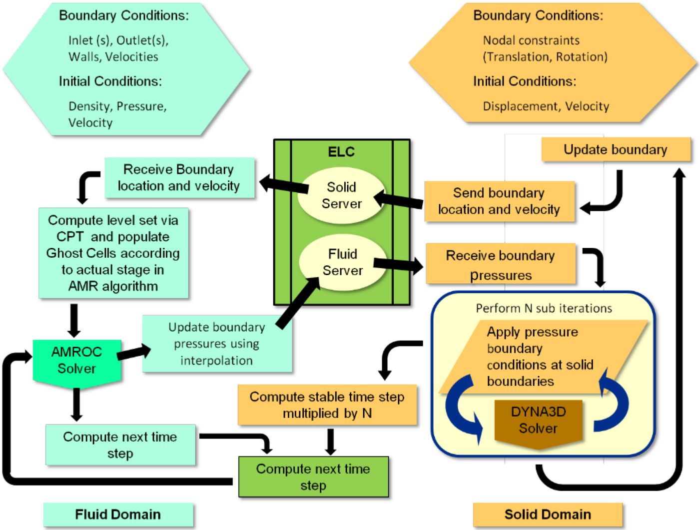

Proximal bodies in hypersonic flow

Flow modeled by Euler equations for a single polytropic gas with $p = (\gamma - 1)\,\rho e$

$$\partial_t \rho + \partial_{x_n}(\rho u_n) = 0\;, \quad \partial_t(\rho u_k) + \partial_{x_n}(\rho u_k u_n + \delta_{kn} p) = 0\;, \quad \partial_t(\rho E) + \partial_{x_n}(u_n(\rho E + p)) = 0$$

Numerical approximation with

- Finite volume flux-vector splitting scheme with MUSCL reconstruction, dimensional splitting

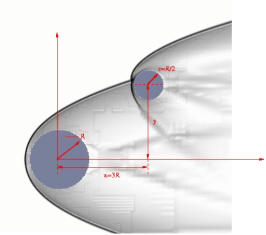

Proximal bodies in hypersonic flow

Flow modeled by Euler equations for a single polytropic gas with $p = (\gamma - 1)\,\rho e$

$$\partial_t \rho + \partial_{x_n}(\rho u_n) = 0\ , \quad \partial_t(\rho u_k) + \partial_{x_n}(\rho u_k u_n + \delta_{kn} p) = 0\ , \quad \partial_t(\rho E) + \partial_{x_n}(u_n(\rho E + p)) = 0$$

Numerical approximation with

- Finite volume flux-vector splitting scheme with MUSCL reconstruction, dimensional splitting
- Spherical bodies, force computation with overlaid lattitude-longitude mesh to obtain drag and lift coefficients $C_{D,L} = \dfrac{2F_{D,L}}{\rho v^2 \pi r^2}$
- inflow $M = 10$, C_D and C_L on secondary sphere, lateral position varied, no motion

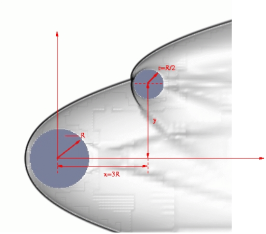

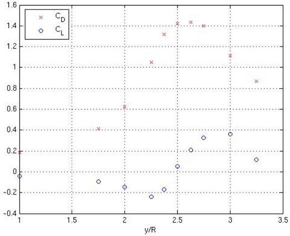

Verification and validation

Static force measurements, $M = 10$:
[Laurence et al., 2007]

- Refinement study: $40 \times 40 \times 32$ base grid , up to without AMR up to $\sim 209.7 \cdot 10^6$ cells, largest run $\sim 35,000\,\mathrm{h}$ CPU

$l_{\max}$	C_D	ΔC_D	C_L	ΔC_L
1	1.264		-0.176	
2	1.442	0.178	-0.019	0.157
3	1.423	-0.019	0.052	0.071
4	1.408	-0.015	0.087	0.035

Verification and validation

Static force measurements, $M = 10$:
[Laurence et al., 2007]

- Refinement study: $40 \times 40 \times 32$ base grid , up to without AMR up to $\sim 209.7 \cdot 10^6$ cells, largest run $\sim 35,000\,\mathrm{h}$ CPU

$l_{\max}$	C_D	ΔC_D	C_L	ΔC_L
1	1.264		-0.176	
2	1.442	0.178	-0.019	0.157
3	1.423	-0.019	0.052	0.071
4	1.408	-0.015	0.087	0.035

- Comparison with experimental results: 3 additional levels, $\sim 2000\,\mathrm{h}$ CPU

	Experimental	Computational
C_D	1.11 ± 0.08	1.01
C_L	0.29 ± 0.05	0.28

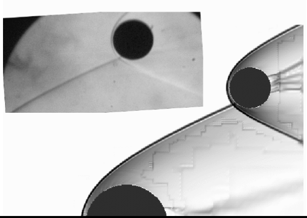

Verification and validation

Static force measurements, $M = 10$:
[Laurence et al., 2007]

- Refinement study: $40 \times 40 \times 32$ base grid , up to without AMR up to $\sim 209.7 \cdot 10^6$ cells, largest run $\sim 35,000\,\mathrm{h}$ CPU

$l_{\max}$	C_D	ΔC_D	C_L	ΔC_L
1	1.264		-0.176	
2	1.442	0.178	-0.019	0.157
3	1.423	-0.019	0.052	0.071
4	1.408	-0.015	0.087	0.035

- Comparison with experimental results: 3 additional levels, $\sim 2000\,\mathrm{h}$ CPU

	Experimental	Computational
C_D	1.11 ± 0.08	1.01
C_L	0.29 ± 0.05	0.28

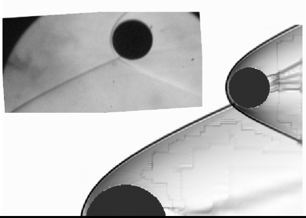

Dynamic motion, $M = 4$:

- Base grid $150 \times 125 \times 90$, two additional levels with $r_{1,2} = 2$
- 24,704 time steps, $36,808\,\mathrm{h}$ CPU on 256 cores IBM BG/P

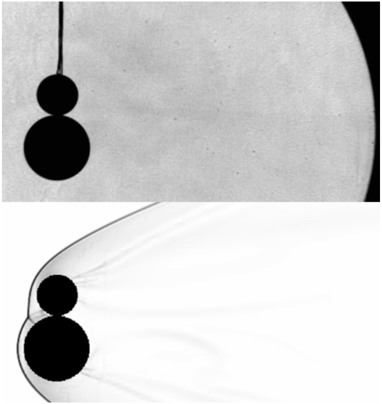

[Laurence and Deiterding, 2011]

Schlieren graphics on refinement regions

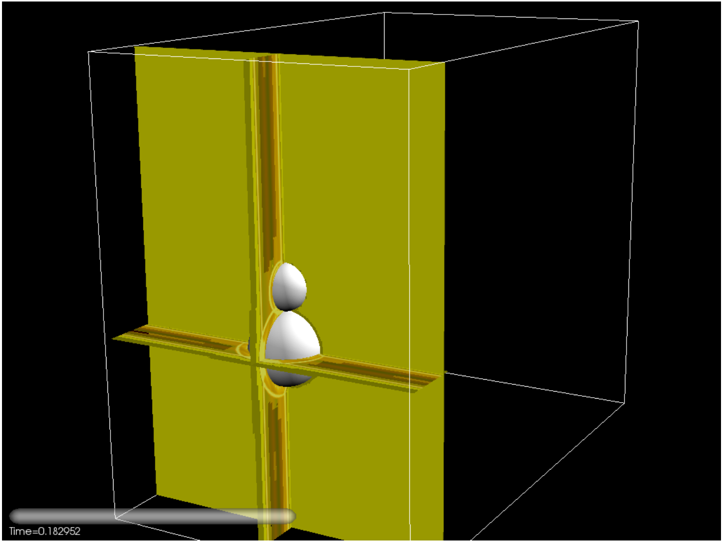

Treatment of thin structures

- Thin boundary structures or lower-dimensional shells require "thickening" to apply embedded boundary method

Treatment of thin structures

- Thin boundary structures or lower-dimensional shells require "thickening" to apply embedded boundary method
- Unsigned distance level set function φ

Treatment of thin structures

- Thin boundary structures or lower-dimensional shells require "thickening" to apply embedded boundary method
- Unsigned distance level set function φ
- Treat cells with $0 < \varphi < d$ as ghost fluid cells

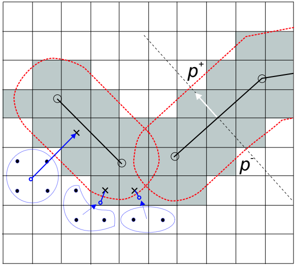

Treatment of thin structures

- Thin boundary structures or lower-dimensional shells require "thickening" to apply embedded boundary method
- Unsigned distance level set function φ
- Treat cells with $0 < \varphi < d$ as ghost fluid cells

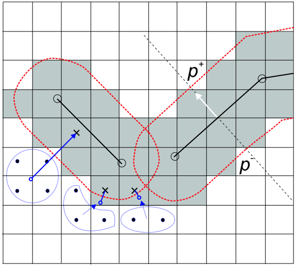

- Leaving φ unmodified ensures correctness of $\nabla\varphi$

Treatment of thin structures

- Thin boundary structures or lower-dimensional shells require "thickening" to apply embedded boundary method
- Unsigned distance level set function φ
- Treat cells with $0 < \varphi < d$ as ghost fluid cells

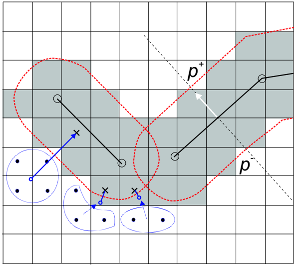

- Leaving φ unmodified ensures correctness of $\nabla\varphi$
- Use face normal in shell element to evaluate in $\Delta p = p^+ - p^-$

Treatment of thin structures

- Thin boundary structures or lower-dimensional shells require "thickening" to apply embedded boundary method
- Unsigned distance level set function φ
- Treat cells with $0 < \varphi < d$ as ghost fluid cells

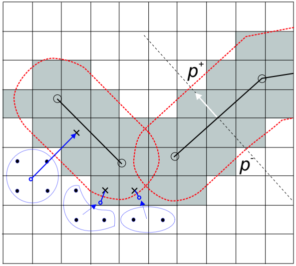

- Leaving φ unmodified ensures correctness of $\nabla\varphi$
- Use face normal in shell element to evaluate in $\Delta p = p^+ - p^-$
- Utilize finite difference solver using the beam equation

$$\rho_s h \frac{\partial^2 w}{\partial t^2} + EI \frac{\partial^4 w}{\partial \bar{x}^4} = p^F$$

to verify FSI algorithms

FSI verification by elastic vibration

- Thin steel plate (thickness $h = 1\,\mathrm{mm}$, length $50\,\mathrm{mm}$), clamped at lower end
- $\rho_s = 7600\,\mathrm{kg/m^3}$, $E = 220\,\mathrm{GPa}$, $I = h^3/12$, $\nu = 0.3$
- Modeled with beam solver (101 points) and thin-shell FEM solver (325 triangles) by F. Cirak

FSI verification by elastic vibration

- Thin steel plate (thickness $h = 1\,\mathrm{mm}$, length $50\,\mathrm{mm}$), clamped at lower end
- $\rho_s = 7600\,\mathrm{kg/m^3}$, $E = 220\,\mathrm{GPa}$, $I = h^3/12$, $\nu = 0.3$
- Modeled with beam solver (101 points) and thin-shell FEM solver (325 triangles) by F. Cirak
- Left: Coupling verification with constant instantenous loading by $\Delta p = 100\,\mathrm{kPa}$

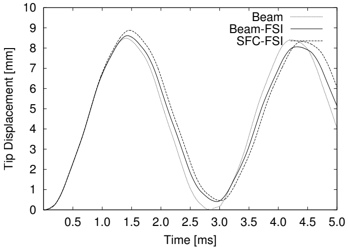

FSI verification by elastic vibration

- Thin steel plate (thickness $h = 1\,\mathrm{mm}$, length $50\,\mathrm{mm}$), clamped at lower end
- $\rho_s = 7600\,\mathrm{kg/m^3}$, $E = 220\,\mathrm{GPa}$, $I = h^3/12$, $\nu = 0.3$
- Modeled with beam solver (101 points) and thin-shell FEM solver (325 triangles) by F. Cirak
- Left: Coupling verification with constant instantenous loading by $\Delta p = 100\,\mathrm{kPa}$
- Right: FSI verification with Mach 1.21 shockwave in air ($\gamma = 1.4$)

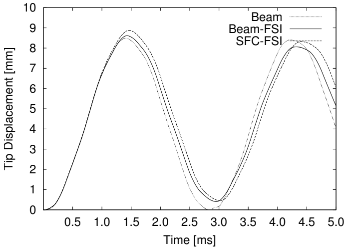

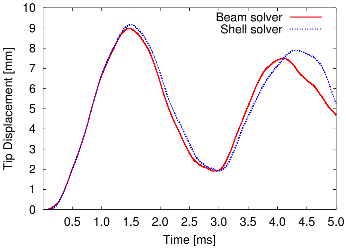

Shock-driven elastic panel motion

Test case suggested by [Giordano et al., 2005]

- Forward facing step geometry, fixed walls everywhere except at inflow

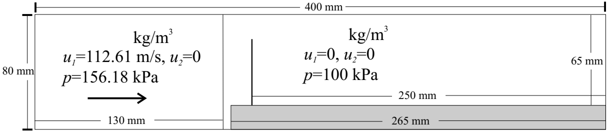

- SAMR base mesh $320 \times 64(\times 2)$, $r_{1,2} = 2$

Shock-driven elastic panel motion

Test case suggested by [Giordano et al., 2005]

- Forward facing step geometry, fixed walls everywhere except at inflow

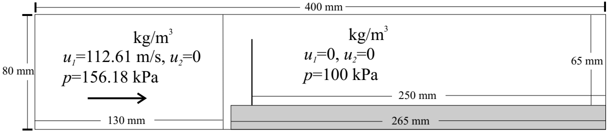

- SAMR base mesh $320 \times 64(\times 2)$, $r_{1,2} = 2$
- Intel 3.4GHz Xeon dual processors, GB Ethernet interconnect
  - Beam-FSI: 12.25 h CPU on 3 fluid CPU + 1 solid CPU
  - FEM-FSI: 322 h CPU on 14 fluid CPU + 2 solid CPU

Shock-driven elastic panel motion

Test case suggested by [Giordano et al., 2005]

- Forward facing step geometry, fixed walls everywhere except at inflow

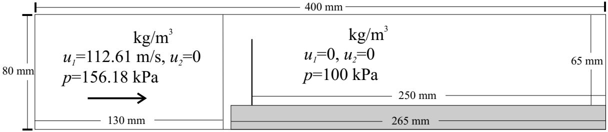

- SAMR base mesh $320 \times 64(\times 2)$, $r_{1,2} = 2$
- Intel 3.4GHz Xeon dual processors, GB Ethernet interconnect
  - Beam-FSI: $12.25\,\mathrm{h}$ CPU on 3 fluid CPU + 1 solid CPU
  - FEM-FSI: $322\,\mathrm{h}$ CPU on 14 fluid CPU + 2 solid CPU

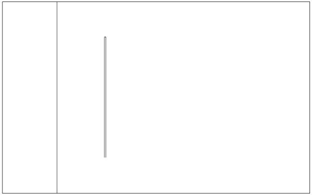

Shock-driven elastic panel motion

Test case suggested by [Giordano et al., 2005]

- Forward facing step geometry, fixed walls everywhere except at inflow

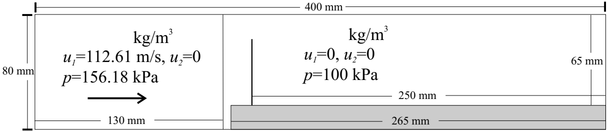

- SAMR base mesh $320 \times 64(\times 2)$, $r_{1,2} = 2$
- Intel 3.4GHz Xeon dual processors, GB Ethernet interconnect
  - Beam-FSI: $12.25\,\mathrm{h}$ CPU on 3 fluid CPU + 1 solid CPU
  - FEM-FSI: $322\,\mathrm{h}$ CPU on 14 fluid CPU + 2 solid CPU

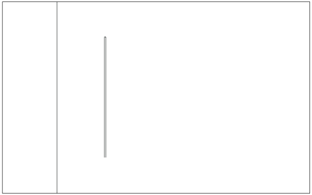

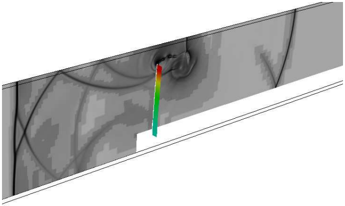

$t = 0.43\,\mathrm{ms}$ after impact

Shock-driven elastic panel motion

Test case suggested by [Giordano et al., 2005]

- Forward facing step geometry, fixed walls everywhere except at inflow

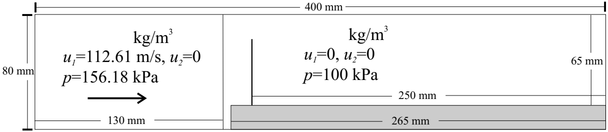

- SAMR base mesh $320 \times 64(\times 2)$, $r_{1,2} = 2$
- Intel 3.4GHz Xeon dual processors, GB Ethernet interconnect
  - Beam-FSI: $12.25\,\mathrm{h}$ CPU on 3 fluid CPU + 1 solid CPU
  - FEM-FSI: $322\,\mathrm{h}$ CPU on 14 fluid CPU + 2 solid CPU

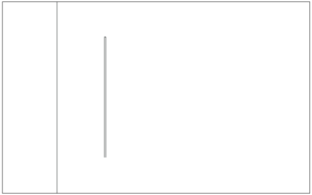

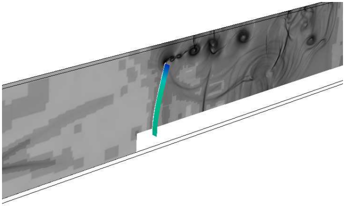

$t = 1.56\,\mathrm{ms}$ after impact

Detonation-driven plastic deformation

Chapman-Jouguet detonation in a tube filled with a stoichiometric ethylene and oxygen ($\mathrm{C_2H_4} + 3\,\mathrm{O_2}$, $295\,\mathrm{K}$) mixture. Euler equations with single exothermic reaction $A \longrightarrow B$

$$\partial_t \rho + \partial_{x_n}(\rho u_n) = 0 \;, \quad \partial_t(\rho u_k) + \partial_{x_n}(\rho u_k u_n + \delta_{kn} p) = 0 \;, k = 1, \ldots, d$$

$$\partial_t(\rho E) + \partial_{x_n}(u_n(\rho E + p)) = 0 \;, \quad \partial_t(Y\rho) + \partial_{x_n}(Y\rho u_n) = \psi$$

with

$$p = (\gamma - 1)(\rho E - \frac{1}{2}\rho u_n u_n - \rho Y q_0) \quad \text{and} \quad \psi = -kY\rho \exp\left(\frac{-E_\mathrm{A}\rho}{p}\right)$$

Detonation-driven plastic deformation

Chapman-Jouguet detonation in a tube filled with a stoichiometric ethylene and oxygen ($\mathrm{C_2H_4} + 3\,\mathrm{O_2}$, $295\,\mathrm{K}$) mixture. Euler equations with single exothermic reaction $A \longrightarrow B$

$$\partial_t \rho + \partial_{x_n}(\rho u_n) = 0\,, \quad \partial_t(\rho u_k) + \partial_{x_n}(\rho u_k u_n + \delta_{kn} p) = 0\,, k = 1, \dots, d$$

$$\partial_t(\rho E) + \partial_{x_n}(u_n(\rho E + p)) = 0\,, \quad \partial_t(Y\rho) + \partial_{x_n}(Y\rho u_n) = \psi$$

with

$$p = (\gamma - 1)(\rho E - \frac{1}{2}\rho u_n u_n - \rho Y q_0) \quad \text{and} \quad \psi = -kY\rho \exp\left(\frac{-E_\mathrm{A}\rho}{p}\right)$$

modeled with heuristic detonation model by [Mader, 1979]

$V := \rho^{-1},\ V_0 := \rho_0^{-1},\ V_\mathrm{CJ} := \rho_\mathrm{CJ}$
$Y' := 1 - (V - V_0)/(V_\mathrm{CJ} - V_0)$
If $0 \le Y' \le 1$ and $Y > 10^{-8}$ then
  If $Y < Y'$ and $Y' < 0.9$ then $Y' := 0$
  If $Y' < 0.99$ then $p' := (1 - Y')p_\mathrm{CJ}$
    else $p' := p$
  $\rho_\mathrm{A} := Y'\rho$
  $E := p'/(\rho(\gamma - 1)) + Y' q_0 + \frac{1}{2} u_n u_n$

Detonation-driven plastic deformation

Chapman-Jouguet detonation in a tube filled with a stoichiometric ethylene and oxygen ($\mathrm{C_2H_4} + 3\,\mathrm{O_2}$, $295\,\mathrm{K}$) mixture. Euler equations with single exothermic reaction $A \longrightarrow B$

$$\partial_t \rho + \partial_{x_n}(\rho u_n) = 0 \;, \quad \partial_t(\rho u_k) + \partial_{x_n}(\rho u_k u_n + \delta_{kn} p) = 0 \;, k = 1, \ldots, d$$

$$\partial_t(\rho E) + \partial_{x_n}(u_n(\rho E + p)) = 0 \;, \quad \partial_t(Y\rho) + \partial_{x_n}(Y\rho u_n) = \psi$$

with

$$p = (\gamma - 1)(\rho E - \frac{1}{2}\rho u_n u_n - \rho Y q_0) \quad \text{and} \quad \psi = -kY\rho \exp\left(\frac{-E_{\mathrm{A}}\rho}{p}\right)$$

modeled with heuristic detonation model by [Mader, 1979]

$V := \rho^{-1},\; V_0 := \rho_0^{-1},\; V_{\mathrm{CJ}} := \rho_{\mathrm{CJ}}$
$Y' := 1 - (V - V_0)/(V_{\mathrm{CJ}} - V_0)$
`If` $0 \le Y' \le 1$ `and` $Y > 10^{-8}$ `then`
  `If` $Y < Y'$ `and` $Y' < 0.9$ `then` $Y' := 0$
  `If` $Y' < 0.99$ `then` $p' := (1 - Y')p_{\mathrm{CJ}}$
    `else` $p' := p$
  $\rho_{\mathrm{A}} := Y'\rho$
  $E := p'/(\rho(\gamma - 1)) + Y' q_0 + \frac{1}{2} u_n u_n$

Comparison of the pressure traces in the experiment and in a 1d simulation

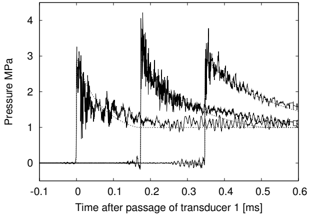

Tube with flaps

- Fluid: VanLeer FVS
  - Detonation model with $\gamma = 1.24$, $p_{\mathrm{CJ}} = 3.3\,\mathrm{MPa}$, $D_{\mathrm{CJ}} = 2376\,\mathrm{m/s}$
  - AMR base level: $104 \times 80 \times 242$, $r_{1,2} = 2$, $r_3 = 4$
  - $\sim 4 \cdot 10^7$ cells instead of $7.9 \cdot 10^9$ cells (uniform)
  - Tube and detonation fully refined
  - Thickening of 2D mesh: $0.81\,\mathrm{mm}$ on both sides (real $0.445\,\mathrm{mm}$)

Tube with flaps

- Fluid: VanLeer FVS
  - Detonation model with $\gamma = 1.24$, $p_{\mathrm{CJ}} = 3.3\,\mathrm{MPa}$, $D_{\mathrm{CJ}} = 2376\,\mathrm{m/s}$
  - AMR base level: $104 \times 80 \times 242$, $r_{1,2} = 2$, $r_3 = 4$
  - $\sim 4 \cdot 10^7$ cells instead of $7.9 \cdot 10^9$ cells (uniform)
  - Tube and detonation fully refined
  - Thickening of 2D mesh: $0.81\,\mathrm{mm}$ on both sides (real $0.445\,\mathrm{mm}$)
- Solid: thin-shell solver by F. Cirak
  - Aluminum, J2 plasticity with hardening, rate sensitivity, and thermal softening
  - Mesh: 8577 nodes, 17056 elements

Tube with flaps

- Fluid: VanLeer FVS
  - Detonation model with $\gamma = 1.24$, $p_{\mathrm{CJ}} = 3.3\,\mathrm{MPa}$, $D_{\mathrm{CJ}} = 2376\,\mathrm{m/s}$
  - AMR base level: $104 \times 80 \times 242$, $r_{1,2} = 2$, $r_3 = 4$
  - $\sim 4 \cdot 10^7$ cells instead of $7.9 \cdot 10^9$ cells (uniform)
  - Tube and detonation fully refined
  - Thickening of 2D mesh: $0.81\,\mathrm{mm}$ on both sides (real $0.445\,\mathrm{mm}$)
- Solid: thin-shell solver by F. Cirak
  - Aluminum, J2 plasticity with hardening, rate sensitivity, and thermal softening
  - Mesh: 8577 nodes, 17056 elements
- 16+2 nodes 2.2 GHz AMD Opteron quad processor, PCI-X 4x Infiniband network, $\sim 4320\,\mathrm{h}$ CPU to $t_{end} = 450\,\mu\mathrm{s}$

Tube with flaps

- Fluid: VanLeer FVS
  - Detonation model with $\gamma = 1.24$, $p_{\rm CJ} = 3.3\,{\rm MPa}$, $D_{\rm CJ} = 2376\,{\rm m/s}$
  - AMR base level: $104 \times 80 \times 242$, $r_{1,2} = 2$, $r_3 = 4$
  - $\sim 4 \cdot 10^7$ cells instead of $7.9 \cdot 10^9$ cells (uniform)
  - Tube and detonation fully refined
  - Thickening of 2D mesh: $0.81\,{\rm mm}$ on both sides (real $0.445\,{\rm mm}$)
- Solid: thin-shell solver by F. Cirak
  - Aluminum, J2 plasticity with hardening, rate sensitivity, and thermal softening
  - Mesh: 8577 nodes, 17056 elements
- 16+2 nodes 2.2 GHz AMD Opteron quad processor, PCI-X 4x Infiniband network, $\sim 4320\,{\rm h}$ CPU to $t_{end} = 450\,\mu{\rm s}$

0.032 ms

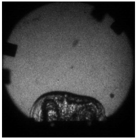

0.030 ms

Tube with flaps

- Fluid: VanLeer FVS
  - Detonation model with $\gamma = 1.24$, $p_{\rm CJ} = 3.3\,\mathrm{MPa}$, $D_{\rm CJ} = 2376\,\mathrm{m/s}$
  - AMR base level: $104 \times 80 \times 242$, $r_{1,2} = 2$, $r_3 = 4$
  - $\sim 4 \cdot 10^7$ cells instead of $7.9 \cdot 10^9$ cells (uniform)
  - Tube and detonation fully refined
  - Thickening of 2D mesh: $0.81\,\mathrm{mm}$ on both sides (real $0.445\,\mathrm{mm}$)
- Solid: thin-shell solver by F. Cirak
  - Aluminum, J2 plasticity with hardening, rate sensitivity, and thermal softening
  - Mesh: 8577 nodes, 17056 elements
- 16+2 nodes 2.2 GHz AMD Opteron quad processor, PCI-X 4x Infiniband network, $\sim 4320\,\mathrm{h}$ CPU to $t_{end} = 450\,\mu\mathrm{s}$


0.032 ms

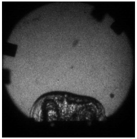
0.030 ms

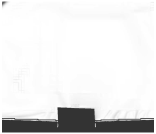
0.212 ms

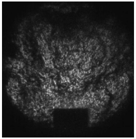
0.210 ms

Tube with flaps: results

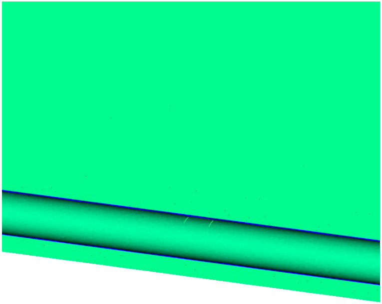

Fluid density and diplacement in y-direction in solid

Tube with flaps: results

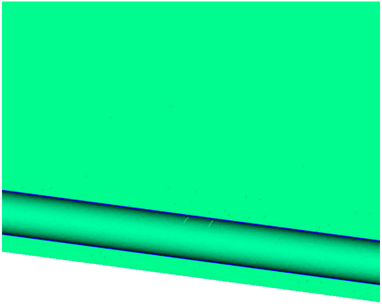

Fluid density and diplacement in y-direction in solid

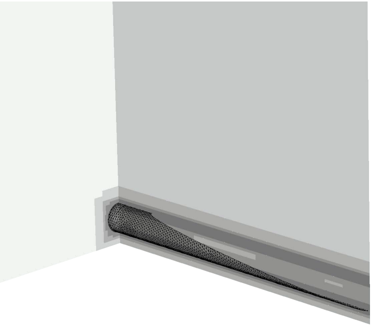

Schlieren plot of fluid density on refinement levels

[Cirak et al., 2007]

Coupled fracture simulation

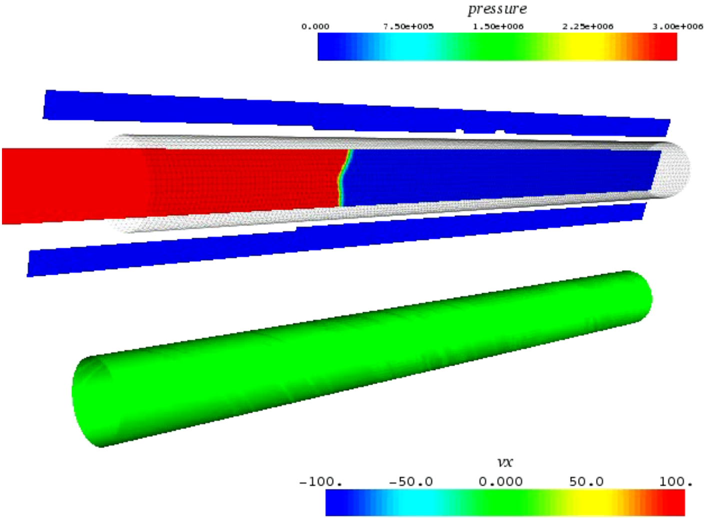

Blast explosion in a multistory building

- $20\,\mathrm{m} \times 40\,\mathrm{m} \times 25\,\mathrm{m}$ seven-story building similar to [Luccioni et al., 2004]
- Spherical energy deposition $\equiv 400\,\mathrm{kg}$ TNT, $r = 0.5\,\mathrm{m}$ in lobby of building
- SAMR: $80 \times 120 \times 90$ base level, three additional levels $r_{1,2} = 2$, $l_{\mathrm{fsi}} = 1$, $k = 1$
- Simulation with ground: 1,070 coupled time steps, $830\,\mathrm{h}$ CPU ($\sim 25.9\,\mathrm{h}$ wall time) on 31+1 cores
- $\sim 8,000,000$ cells instead of $55,296,000$ (uniform)
- 69,709 hexahedral elements and with material parameters. [Deiterding and Wood, 2013]

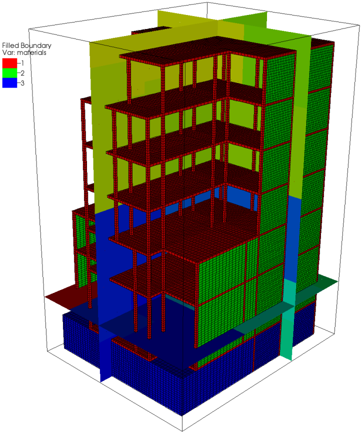

	ρ_s [kg/m^3]	σ_0 [MPa]	E_T [GPa]	β	K [GPa]	G [GPa]	$\bar{\epsilon}^p$	p_f [MPa]
Columns	2010	50	11.2	1.0	21.72	4.67	0.02	-30
Walls	2010	25	11.2	1.0	6.22	4.67	0.01	-15

Blast explosion in a multistory building

- $20\,\mathrm{m} \times 40\,\mathrm{m} \times 25\,\mathrm{m}$ seven-story building similar to [Luccioni et al., 2004]
- Spherical energy deposition $\equiv 400\,\mathrm{kg}$ TNT, $r = 0.5\,\mathrm{m}$ in lobby of building
- SAMR: $80 \times 120 \times 90$ base level, three additional levels $r_{1,2} = 2$, $l_{\mathrm{fsi}} = 1$, $k = 1$
- Simulation with ground: $1,070$ coupled time steps, $830\,\mathrm{h}$ CPU ($\sim 25.9\,\mathrm{h}$ wall time) on 31+1 cores
- $\sim 8,000,000$ cells instead of $55,296,000$ (uniform)
- $69,709$ hexahedral elements and with material parameters. [Deiterding and Wood, 2013]

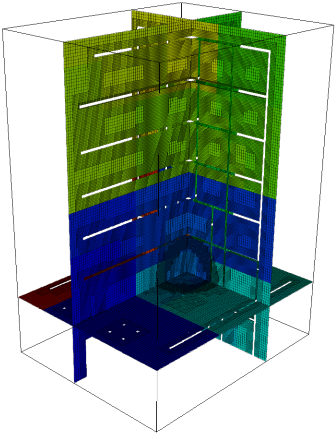

	ρ_s [kg/m^3]	σ_0 [MPa]	E_T [GPa]	β	K [GPa]	G [GPa]	$\bar{\epsilon}^p$	p_f [MPa]
Columns	2010	50	11.2	1.0	21.72	4.67	0.02	-30
Walls	2010	25	11.2	1.0	6.22	4.67	0.01	-15

Blast explosion in a multistory building

- $20\,\mathrm{m} \times 40\,\mathrm{m} \times 25\,\mathrm{m}$ seven-story building similar to [Luccioni et al., 2004]
- Spherical energy deposition $\equiv 400\,\mathrm{kg}$ TNT, $r = 0.5\,\mathrm{m}$ in lobby of building
- SAMR: $80 \times 120 \times 90$ base level, three additional levels $r_{1,2} = 2$, $l_{\mathrm{fsi}} = 1$, $k = 1$
- Simulation with ground: $1,070$ coupled time steps, $830\,\mathrm{h}$ CPU ($\sim 25.9\,\mathrm{h}$ wall time) on 31+1 cores
- $\sim 8,000,000$ cells instead of $55,296,000$ (uniform)
- $69,709$ hexahedral elements and with material parameters. [Deiterding and Wood, 2013]

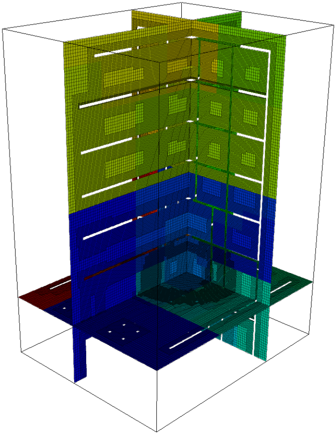

	ρ_s [kg/m^3]	σ_0 [MPa]	E_T [GPa]	β	K [GPa]	G [GPa]	$\bar{\epsilon}^p$	p_f [MPa]
Columns	2010	50	11.2	1.0	21.72	4.67	0.02	-30
Walls	2010	25	11.2	1.0	6.22	4.67	0.01	-15

Blast explosion in a multistory building

- $20\,\mathrm{m} \times 40\,\mathrm{m} \times 25\,\mathrm{m}$ seven-story building similar to [Luccioni et al., 2004]
- Spherical energy deposition $\equiv 400\,\mathrm{kg}$ TNT, $r = 0.5\,\mathrm{m}$ in lobby of building
- SAMR: $80 \times 120 \times 90$ base level, three additional levels $r_{1,2} = 2$, $l_{\mathrm{fsi}} = 1$, $k = 1$
- Simulation with ground: 1,070 coupled time steps, $830\,\mathrm{h}$ CPU ($\sim 25.9\,\mathrm{h}$ wall time) on 31+1 cores
- $\sim$ 8,000,000 cells instead of 55,296,000 (uniform)
- 69,709 hexahedral elements and with material parameters. [Deiterding and Wood, 2013]

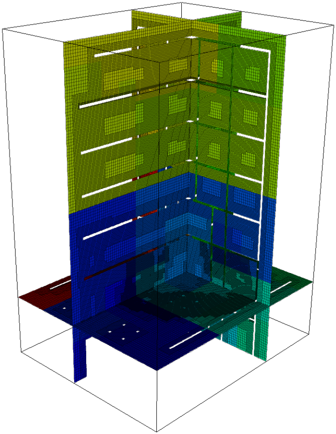

	ρ_s [kg/m^3]	σ_0 [MPa]	E_T [GPa]	β	K [GPa]	G [GPa]	$\bar{\epsilon}^p$	p_f [MPa]
Columns	2010	50	11.2	1.0	21.72	4.67	0.02	-30
Walls	2010	25	11.2	1.0	6.22	4.67	0.01	-15

Blast explosion in a multistory building

- $20\,\mathrm{m} \times 40\,\mathrm{m} \times 25\,\mathrm{m}$ seven-story building similar to [Luccioni et al., 2004]
- Spherical energy deposition $\equiv 400\,\mathrm{kg}$ TNT, $r = 0.5\,\mathrm{m}$ in lobby of building
- SAMR: $80 \times 120 \times 90$ base level, three additional levels $r_{1,2} = 2$, $l_{\mathrm{fsi}} = 1$, $k = 1$
- Simulation with ground: $1,070$ coupled time steps, $830\,\mathrm{h}$ CPU ($\sim 25.9\,\mathrm{h}$ wall time) on 31+1 cores
- $\sim 8,000,000$ cells instead of $55,296,000$ (uniform)
- $69,709$ hexahedral elements and with material parameters. [Deiterding and Wood, 2013]

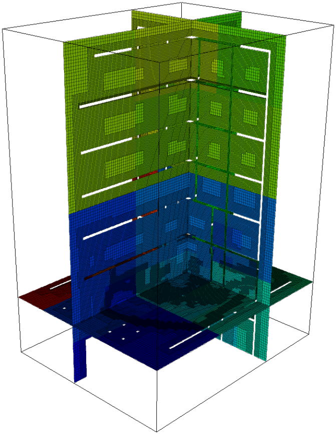

	ρ_s [kg/m^3]	σ_0 [MPa]	E_T [GPa]	β	K [GPa]	G [GPa]	$\bar{\epsilon}^p$	p_f [MPa]
Columns	2010	50	11.2	1.0	21.72	4.67	0.02	-30
Walls	2010	25	11.2	1.0	6.22	4.67	0.01	-15

Blast explosion in a multistory building

- $20\,\mathrm{m} \times 40\,\mathrm{m} \times 25\,\mathrm{m}$ seven-story building similar to [Luccioni et al., 2004]
- Spherical energy deposition $\equiv 400\,\mathrm{kg}$ TNT, $r = 0.5\,\mathrm{m}$ in lobby of building
- SAMR: $80 \times 120 \times 90$ base level, three additional levels $r_{1,2} = 2$, $l_{\mathrm{fsi}} = 1$, $k = 1$
- Simulation with ground: $1,070$ coupled time steps, $830\,\mathrm{h}$ CPU ($\sim 25.9\,\mathrm{h}$ wall time) on 31+1 cores
- $\sim 8,000,000$ cells instead of $55,296,000$ (uniform)
- $69,709$ hexahedral elements and with material parameters. [Deiterding and Wood, 2013]

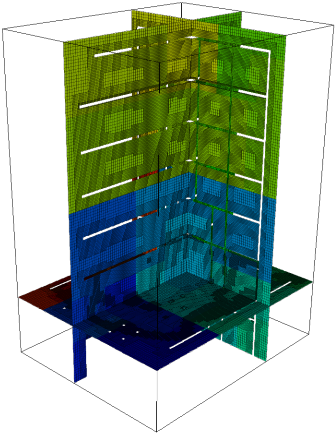

	ρ_s [kg/m^3]	σ_0 [MPa]	E_T [GPa]	β	K [GPa]	G [GPa]	$\bar{\epsilon}^p$	p_f [MPa]
Columns	2010	50	11.2	1.0	21.72	4.67	0.02	-30
Walls	2010	25	11.2	1.0	6.22	4.67	0.01	-15

Blast explosion in a multistory building

- $20\,\mathrm{m} \times 40\,\mathrm{m} \times 25\,\mathrm{m}$ seven-story building similar to [Luccioni et al., 2004]
- Spherical energy deposition $\equiv 400\,\mathrm{kg}$ TNT, $r = 0.5\,\mathrm{m}$ in lobby of building
- SAMR: $80 \times 120 \times 90$ base level, three additional levels $r_{1,2} = 2$, $l_{\mathrm{fsi}} = 1$, $k = 1$
- Simulation with ground: $1,070$ coupled time steps, $830\,\mathrm{h}$ CPU ($\sim 25.9\,\mathrm{h}$ wall time) on 31+1 cores
- $\sim 8,000,000$ cells instead of $55,296,000$ (uniform)
- $69,709$ hexahedral elements and with material parameters. [Deiterding and Wood, 2013]

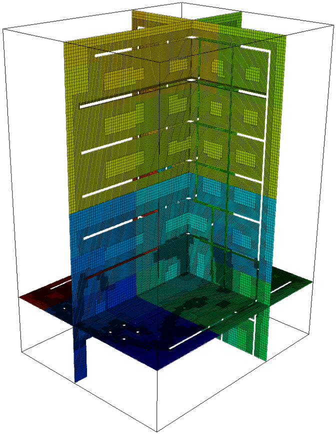

	ρ_s [kg/m^3]	σ_0 [MPa]	E_T [GPa]	β	K [GPa]	G [GPa]	$\bar{\epsilon}^p$	p_f [MPa]
Columns	2010	50	11.2	1.0	21.72	4.67	0.02	-30
Walls	2010	25	11.2	1.0	6.22	4.67	0.01	-15

Blast explosion in a multistory building

- $20\,\mathrm{m} \times 40\,\mathrm{m} \times 25\,\mathrm{m}$ seven-story building similar to [Luccioni et al., 2004]
- Spherical energy deposition $\equiv 400\,\mathrm{kg}$ TNT, $r = 0.5\,\mathrm{m}$ in lobby of building
- SAMR: $80 \times 120 \times 90$ base level, three additional levels $r_{1,2} = 2$, $l_{\mathrm{fsi}} = 1$, $k = 1$
- Simulation with ground: $1,070$ coupled time steps, $830\,\mathrm{h}$ CPU ($\sim 25.9\,\mathrm{h}$ wall time) on 31+1 cores
- $\sim 8,000,000$ cells instead of $55,296,000$ (uniform)
- $69,709$ hexahedral elements and with material parameters. [Deiterding and Wood, 2013]

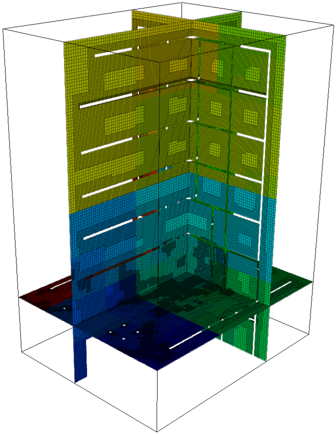

	ρ_s [kg/m^3]	σ_0 [MPa]	E_T [GPa]	β	K [GPa]	G [GPa]	$\bar{\epsilon}^p$	p_f [MPa]
Columns	2010	50	11.2	1.0	21.72	4.67	0.02	-30
Walls	2010	25	11.2	1.0	6.22	4.67	0.01	-15

Blast explosion in a multistory building

- $20\,\mathrm{m} \times 40\,\mathrm{m} \times 25\,\mathrm{m}$ seven-story building similar to [Luccioni et al., 2004]
- Spherical energy deposition $\equiv 400\,\mathrm{kg}$ TNT, $r = 0.5\,\mathrm{m}$ in lobby of building
- SAMR: $80 \times 120 \times 90$ base level, three additional levels $r_{1,2} = 2$, $l_{\mathrm{fsi}} = 1$, $k = 1$
- Simulation with ground: 1,070 coupled time steps, $830\,\mathrm{h}$ CPU ($\sim 25.9\,\mathrm{h}$ wall time) on 31+1 cores
- $\sim 8,000,000$ cells instead of $55,296,000$ (uniform)
- 69,709 hexahedral elements and with material parameters. [Deiterding and Wood, 2013]

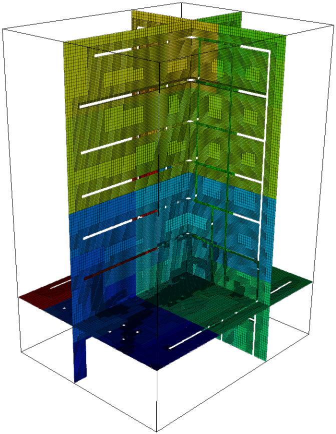

	ρ_s [kg/m^3]	σ_0 [MPa]	E_T [GPa]	β	K [GPa]	G [GPa]	$\bar{\epsilon}^p$	p_f [MPa]
Columns	2010	50	11.2	1.0	21.72	4.67	0.02	-30
Walls	2010	25	11.2	1.0	6.22	4.67	0.01	-15

Blast explosion in a multistory building

- $20\,\mathrm{m} \times 40\,\mathrm{m} \times 25\,\mathrm{m}$ seven-story building similar to [Luccioni et al., 2004]
- Spherical energy deposition $\equiv 400\,\mathrm{kg}$ TNT, $r = 0.5\,\mathrm{m}$ in lobby of building
- SAMR: $80 \times 120 \times 90$ base level, three additional levels $r_{1,2} = 2$, $l_{\mathrm{fsi}} = 1$, $k = 1$
- Simulation with ground: 1,070 coupled time steps, $830\,\mathrm{h}$ CPU ($\sim 25.9\,\mathrm{h}$ wall time) on 31+1 cores
- $\sim 8,000,000$ cells instead of $55,296,000$ (uniform)
- 69,709 hexahedral elements and with material parameters. [Deiterding and Wood, 2013]

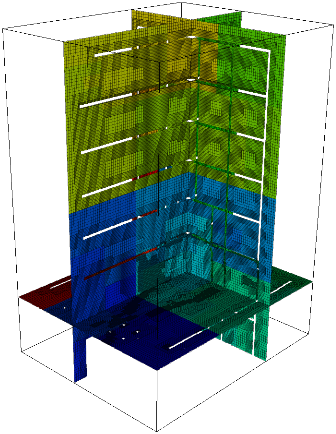

	ρ_s [kg/m^3]	σ_0 [MPa]	E_T [GPa]	β	K [GPa]	G [GPa]	$\bar{\epsilon}^p$	p_f [MPa]
Columns	2010	50	11.2	1.0	21.72	4.67	0.02	-30
Walls	2010	25	11.2	1.0	6.22	4.67	0.01	-15

Blast explosion in a multistory building

- $20\,\mathrm{m} \times 40\,\mathrm{m} \times 25\,\mathrm{m}$ seven-story building similar to [Luccioni et al., 2004]
- Spherical energy deposition $\equiv 400\,\mathrm{kg}$ TNT, $r = 0.5\,\mathrm{m}$ in lobby of building
- SAMR: $80 \times 120 \times 90$ base level, three additional levels $r_{1,2} = 2$, $l_{\mathrm{fsi}} = 1$, $k = 1$
- Simulation with ground: 1,070 coupled time steps, $830\,\mathrm{h}$ CPU ($\sim 25.9\,\mathrm{h}$ wall time) on 31+1 cores
- $\sim 8,000,000$ cells instead of $55,296,000$ (uniform)
- 69,709 hexahedral elements and with material parameters. [Deiterding and Wood, 2013]

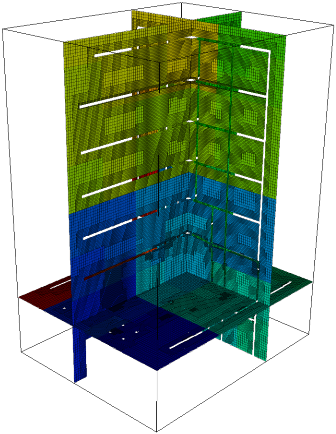

	ρ_s [kg/m^3]	σ_0 [MPa]	E_T [GPa]	β	K [GPa]	G [GPa]	$\bar{\epsilon}^p$	p_f [MPa]
Columns	2010	50	11.2	1.0	21.72	4.67	0.02	-30
Walls	2010	25	11.2	1.0	6.22	4.67	0.01	-15

Blast explosion in a multistory building

- $20\,\mathrm{m} \times 40\,\mathrm{m} \times 25\,\mathrm{m}$ seven-story building similar to [Luccioni et al., 2004]
- Spherical energy deposition $\equiv 400\,\mathrm{kg}$ TNT, $r = 0.5\,\mathrm{m}$ in lobby of building
- SAMR: $80 \times 120 \times 90$ base level, three additional levels $r_{1,2} = 2$, $l_{\mathrm{fsi}} = 1$, $k = 1$
- Simulation with ground: $1,070$ coupled time steps, $830\,\mathrm{h}$ CPU ($\sim 25.9\,\mathrm{h}$ wall time) on 31+1 cores
- $\sim 8,000,000$ cells instead of $55,296,000$ (uniform)
- $69,709$ hexahedral elements and with material parameters. [Deiterding and Wood, 2013]

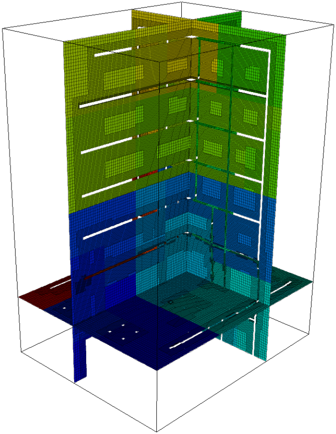

	ρ_s [kg/m^3]	σ_0 [MPa]	E_T [GPa]	β	K [GPa]	G [GPa]	$\bar{\epsilon}^p$	p_f [MPa]
Columns	2010	50	11.2	1.0	21.72	4.67	0.02	-30
Walls	2010	25	11.2	1.0	6.22	4.67	0.01	-15

Blast explosion in a multistory building

- $20\,\mathrm{m} \times 40\,\mathrm{m} \times 25\,\mathrm{m}$ seven-story building similar to [Luccioni et al., 2004]
- Spherical energy deposition $\equiv 400\,\mathrm{kg}$ TNT, $r = 0.5\,\mathrm{m}$ in lobby of building
- SAMR: $80 \times 120 \times 90$ base level, three additional levels $r_{1,2} = 2$, $l_{\mathrm{fsi}} = 1$, $k = 1$
- Simulation with ground: $1,070$ coupled time steps, $830\,\mathrm{h}$ CPU ($\sim 25.9\,\mathrm{h}$ wall time) on 31+1 cores
- $\sim 8,000,000$ cells instead of $55,296,000$ (uniform)
- $69,709$ hexahedral elements and with material parameters. [Deiterding and Wood, 2013]

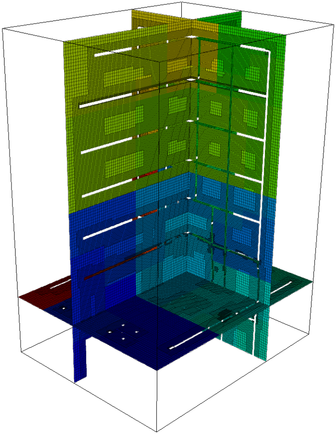

	ρ_s [kg/m^3]	σ_0 [MPa]	E_T [GPa]	β	K [GPa]	G [GPa]	$\bar{\epsilon}^p$	p_f [MPa]
Columns	2010	50	11.2	1.0	21.72	4.67	0.02	-30
Walls	2010	25	11.2	1.0	6.22	4.67	0.01	-15

Blast explosion in a multistory building

- $20\,\mathrm{m} \times 40\,\mathrm{m} \times 25\,\mathrm{m}$ seven-story building similar to [Luccioni et al., 2004]
- Spherical energy deposition $\equiv 400\,\mathrm{kg}$ TNT, $r = 0.5\,\mathrm{m}$ in lobby of building
- SAMR: $80 \times 120 \times 90$ base level, three additional levels $r_{1,2} = 2$, $l_{\rm fsi} = 1$, $k = 1$
- Simulation with ground: $1,070$ coupled time steps, $830\,\mathrm{h}$ CPU ($\sim 25.9\,\mathrm{h}$ wall time) on 31+1 cores
- $\sim 8,000,000$ cells instead of $55,296,000$ (uniform)
- $69,709$ hexahedral elements and with material parameters. [Deiterding and Wood, 2013]

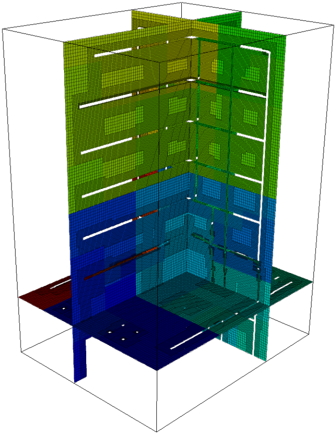

	ρ_s [kg/m^3]	σ_0 [MPa]	E_T [GPa]	β	K [GPa]	G [GPa]	$\bar{\epsilon}^p$	p_f [MPa]
Columns	2010	50	11.2	1.0	21.72	4.67	0.02	-30
Walls	2010	25	11.2	1.0	6.22	4.67	0.01	-15

Blast explosion in a multistory building – II

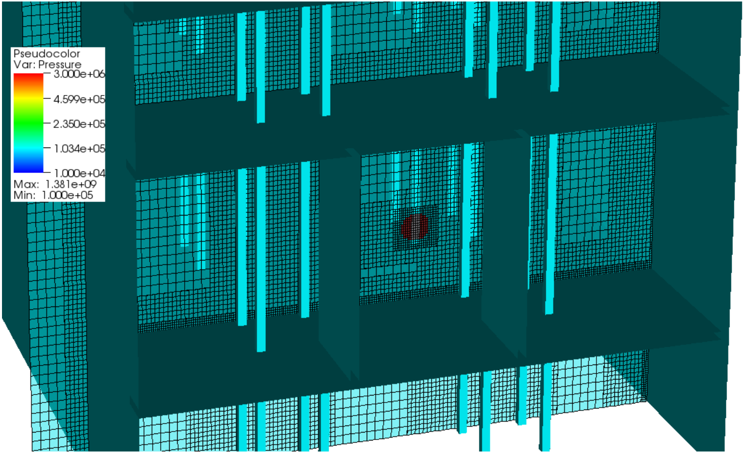

$t = 0$

Blast explosion in a multistory building – II

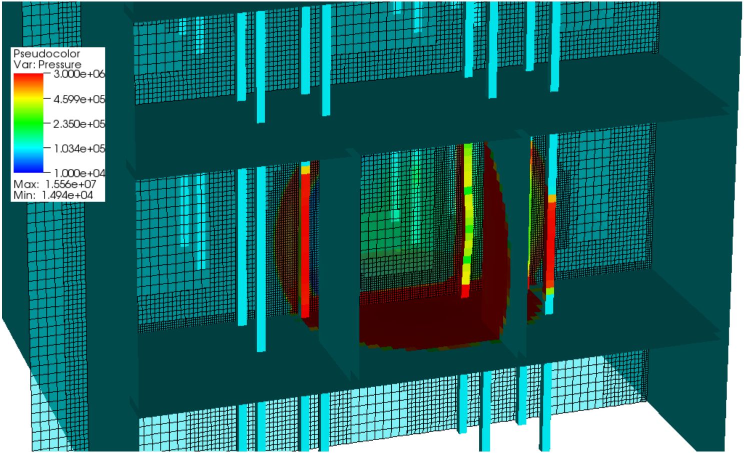

Blast explosion in a multistory building – II

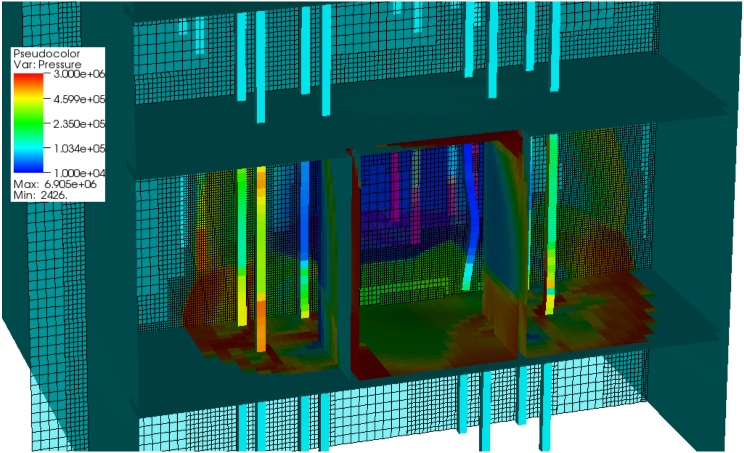

$t = 6.1\,\mathrm{ms}$

Blast explosion in a multistory building – II

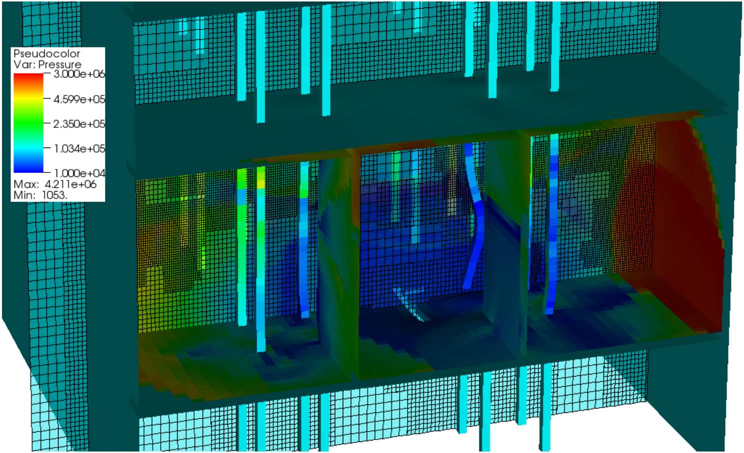

Blast explosion in a multistory building – II

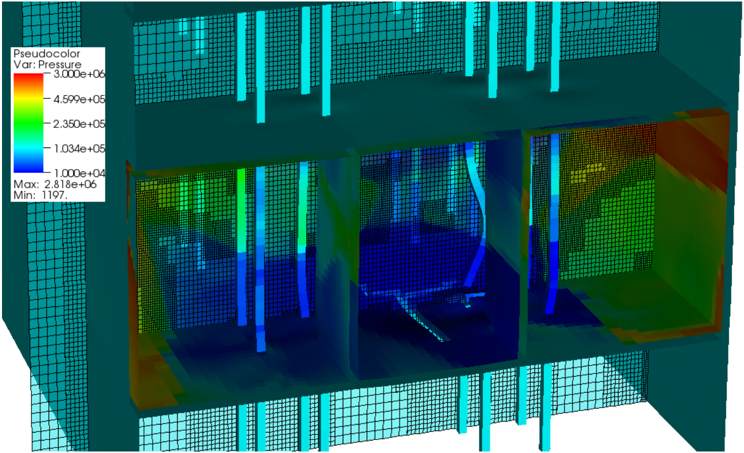

Blast explosion in a multistory building – II

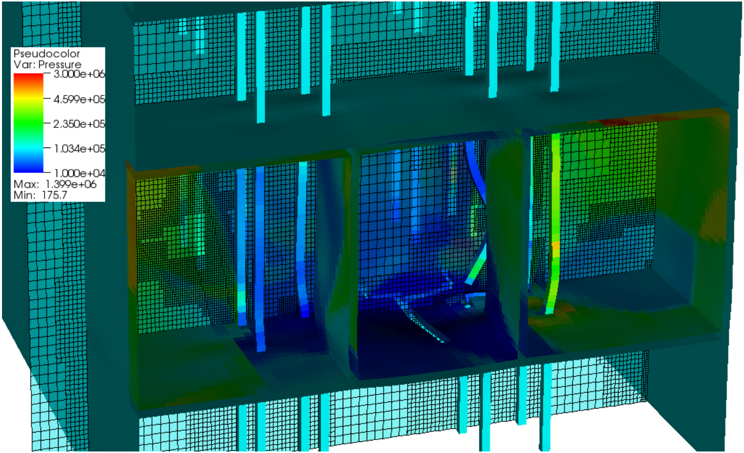

Blast explosion in a multistory building – II

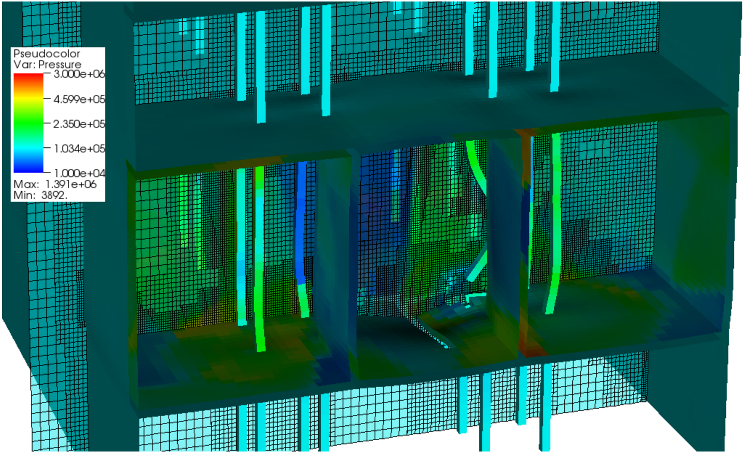

Blast explosion in a multistory building – II

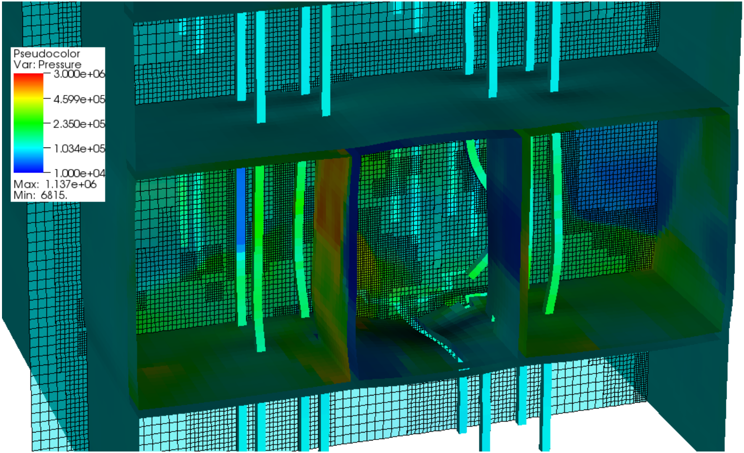

Blast explosion in a multistory building – II

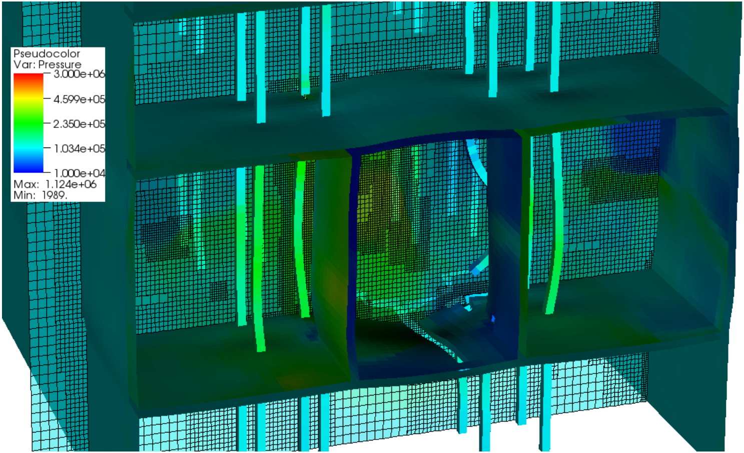

$t = 29.2\,\mathrm{ms}$

Blast explosion in a multistory building – II

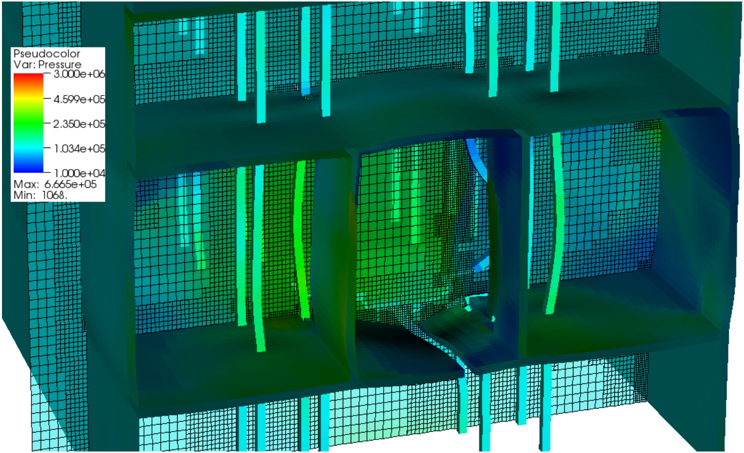

Blast explosion in a multistory building – II

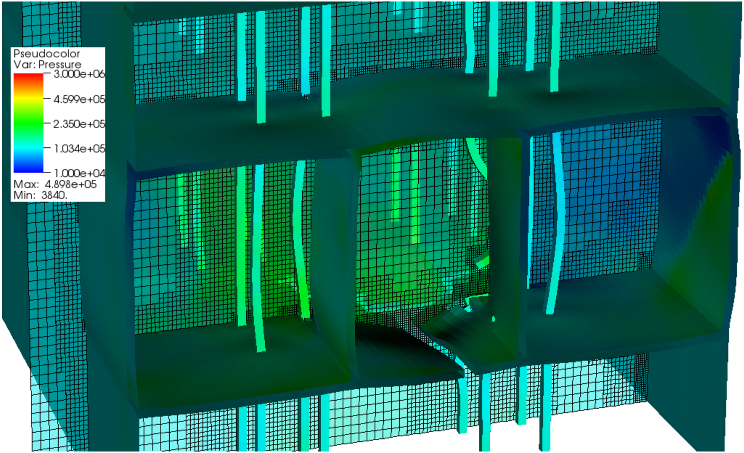

Blast explosion in a multistory building – II

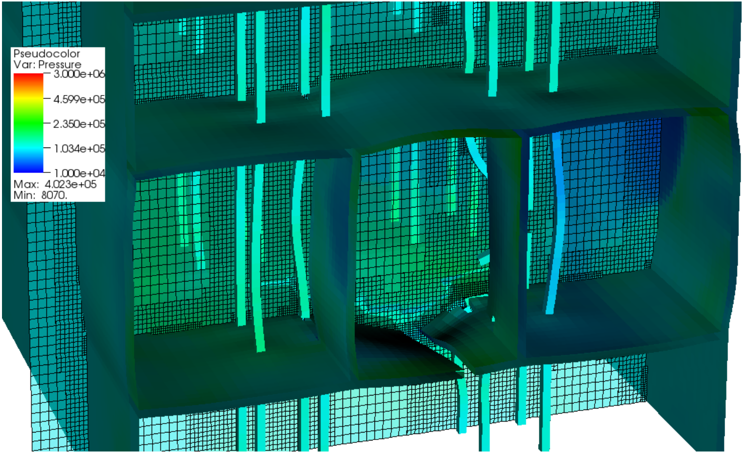

Blast explosion in a multistory building – II

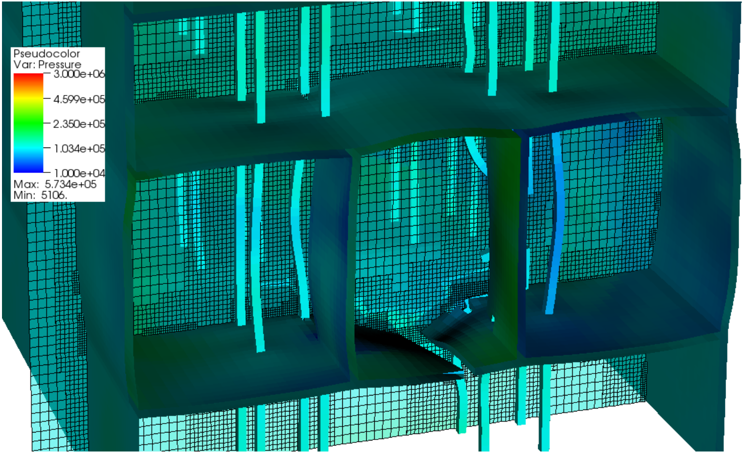

Blast explosion in a multistory building – II

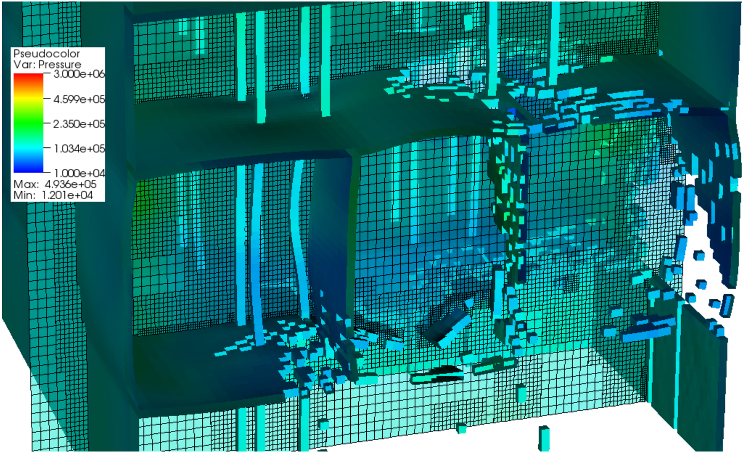

$t = 48.7\,\mathrm{ms}$

Laboratory tunnel simulator [Zonglin et al., 2002]

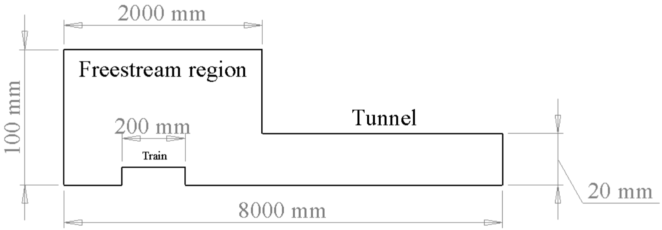

Laboratory tunnel simulator [Zonglin et al., 2002]

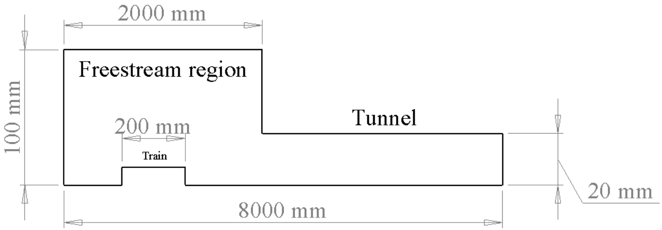

Model solves the inviscid Euler equations

$$\begin{aligned}\partial_t \rho + \nabla \cdot (\rho \mathbf{u}) = 0 \\ \partial_t (\rho \mathbf{u}) + \nabla \cdot (\rho \mathbf{u} \otimes \mathbf{u}) + \nabla p = 0 \\ \partial_t (\rho E) + \nabla \cdot ((\rho E + p)\mathbf{u}) = 0\end{aligned}$$

with $p = (\gamma - 1)(\rho E - \frac{1}{2}\rho \mathbf{u}^T \mathbf{u})$

Laboratory tunnel simulator [Zonglin et al., 2002]

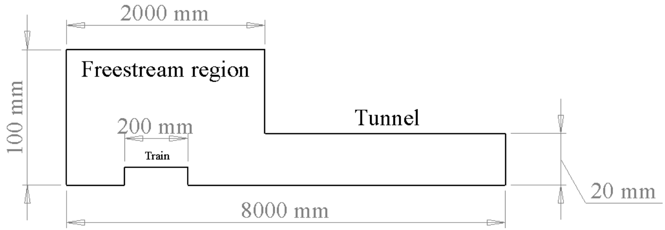

Model solves the inviscid Euler equations

$$\partial_t \rho + \nabla \cdot (\rho \mathbf{u}) = 0$$
$$\partial_t(\rho \mathbf{u}) + \nabla \cdot (\rho \mathbf{u} \otimes \mathbf{u}) + \nabla p = 0$$
$$\partial_t(\rho E) + \nabla \cdot ((\rho E + p)\mathbf{u}) = 0$$

with $p = (\gamma - 1)(\rho E - \frac{1}{2}\rho \mathbf{u}^T \mathbf{u})$

- Two-dimensional axi-symmetric computation
- $p_0 = 100\,\mathrm{kPa}$, $\rho_0 = 1.225\,\mathrm{kg/m^3}$, $\gamma = 1.4$
- Roe shock-capturing scheme blended with HLL
- 2nd order accuracy achieved with MUSCL-Hancock method

Basic phenomena – $v_0 = 100\,\mathrm{m/s}$

- 800×25 mesh with Cartesian cut-out $(200, 5)$ to $(800, 25)$
- 2 level of additional refinement by factor 2

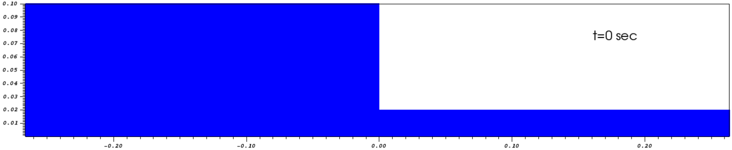

Basic phenomena – $v_0 = 100\,\mathrm{m/s}$

- 800×25 mesh with Cartesian cut-out $(200, 5)$ to $(800, 25)$
- 2 level of additional refinement by factor 2

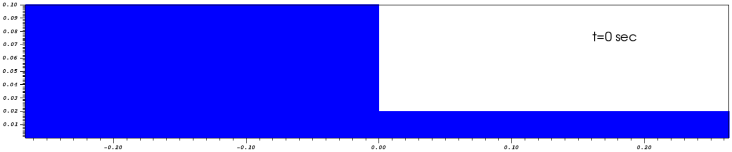

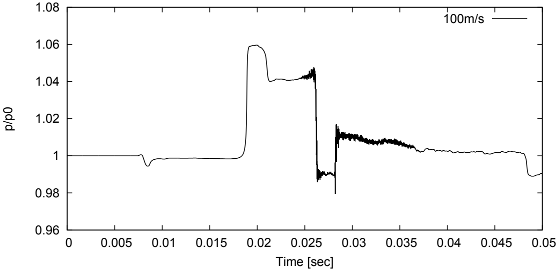

Pressure record at location $(1020\,\mathrm{mm}, 20\,\mathrm{mm})$ inside tunnel

Comparison with experiment – I

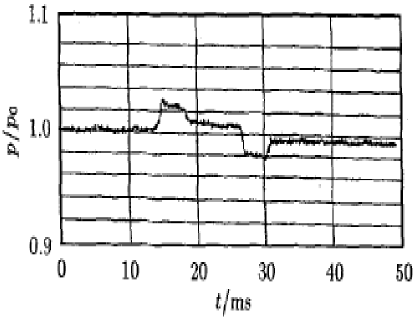

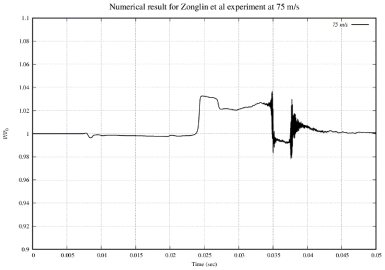

Pressure record at ($1020\,\mathrm{mm}, 20\,\mathrm{mm}$) for $v_0 = 75\,\mathrm{m/s}$. Experiment (left) and AMROC (right)

Comparison with experiment – I

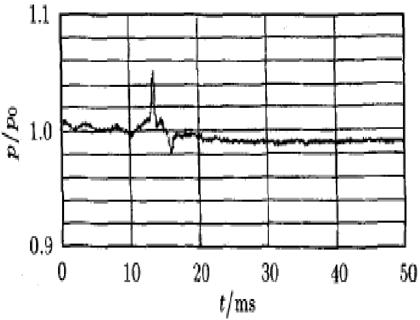

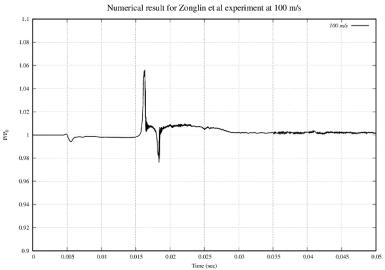

Pressure record at $(40\,\mathrm{mm}, 20\,\mathrm{mm})$ for model velocity $v_0 = 100\,\mathrm{m/s}$. Experiment (left) and AMROC (right)

Variation of velocity and nose half angle

Pressure sensor at $(420\,\mathrm{mm}, 20\,\mathrm{mm})$

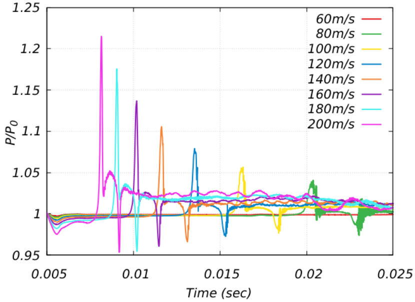

Pressure sensor at $(1020\,\mathrm{mm}, 20\,\mathrm{mm})$

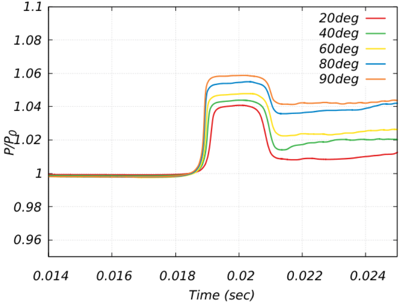

- Dependence on v_0^2 is the dynamic pressure influence (left)
- For constant blockage ratio and body velocity, using more pointed noses alleviates the maximal pressure level (right, nose half angle varied)
- For $v_0 \approx 140\,\mathrm{m/s}$ a shock wave (tunnel boom) can be observed. Sharper noses also delay this phenomenon.

NGT2 prototype setup

- Next Generation Train 2 (NGT2) geometry by the German Aerospace Centre (DLR) [Fragner and Deiterding, 2016, Fragner and Deiterding, 2017]
- Mirrored train head of length $\sim 60\,\mathrm{m}$, no wheels or tracks, train models $0.17\,\mathrm{m}$ above ground above the ground level.
- Train velocities $100\,\mathrm{m/s}$ and $-100\,\mathrm{m/s}$, middle axis $6\,\mathrm{m}$ apart, initial distance between centers $200\,\mathrm{m}$
- Base mesh of $360 \times 40 \times 30$ for domain of $360\,\mathrm{m} \times 40\,\mathrm{m} \times 30\,\mathrm{m}$
- Two/three additional levels, refined by $r_{1,2,3} = 2$. Refinement based on pressure gradient and level set and regenerated at every coarse time step. Parallel redistribution at every level-0 time step.
- On 96 cores Intel Xeon E5-2670 $2.6\,\mathrm{GHz}$ a final $t_e = 3\,\mathrm{sec}$ was reached after $12,385\,\mathrm{sec}$ / $43,395\,\mathrm{sec}$ wall time, i.e., $330\,\mathrm{h}$ and $1157\,\mathrm{h}$ CPU

Passing in open space – AMR and dynamic distribution

Domains of three-level refinement

Distribution to 96 processors

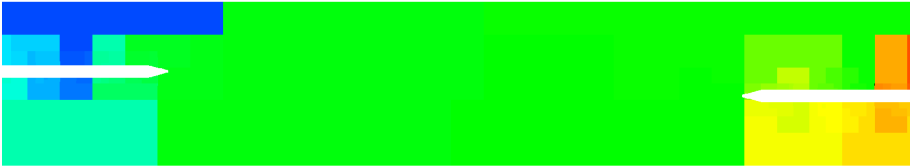

Enlargement of domain center shown

Passing in open space – AMR and dynamic distribution

Domains of three-level refinement

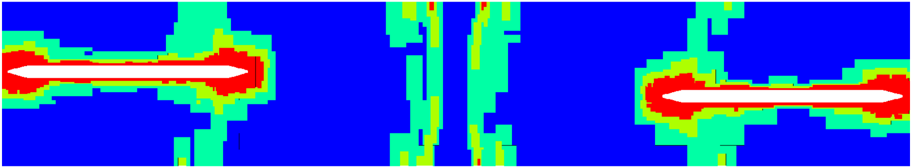

Distribution to 96 processors

Enlargement of domain center shown

Passing in open space – AMR and dynamic distribution

Domains of three-level refinement

Distribution to 96 processors

Enlargement of domain center shown

Passing in open space – AMR and dynamic distribution

Domains of three-level refinement

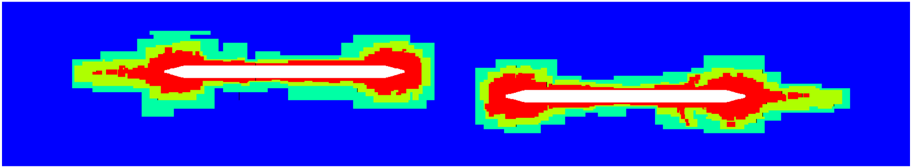

Distribution to 96 processors

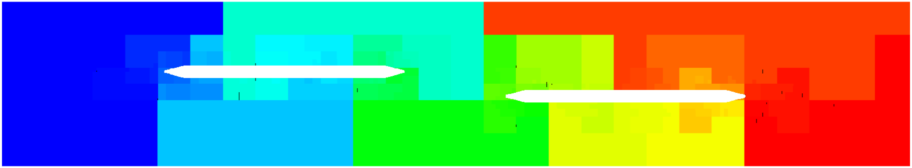

Enlargement of domain center shown

Passing in open space – AMR and dynamic distribution

Domains of three-level refinement

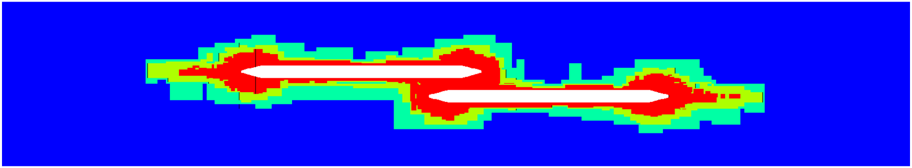

Distribution to 96 processors

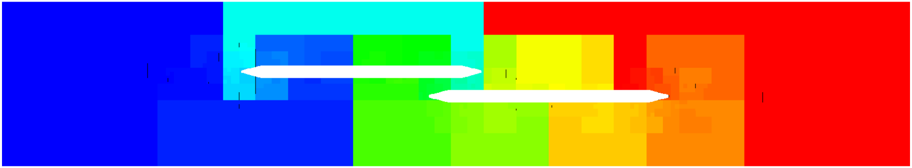

Enlargement of domain center shown

Passing in open space – AMR and dynamic distribution

Domains of three-level refinement

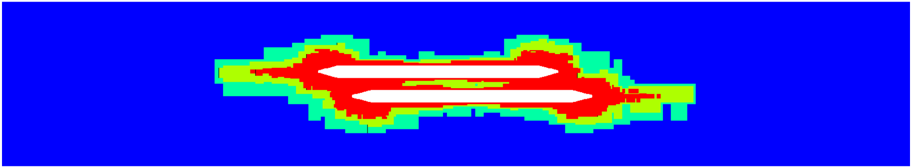

Distribution to 96 processors

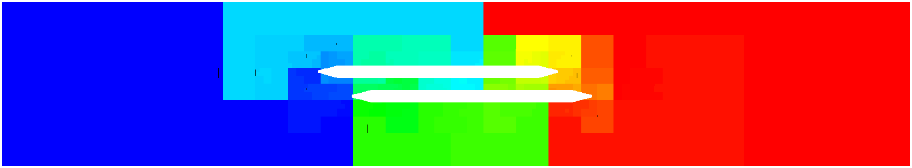

Enlargement of domain center shown

Passing in open space – AMR and dynamic distribution

Domains of three-level refinement

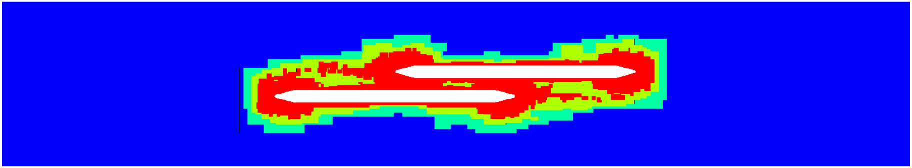

Distribution to 96 processors

Enlargement of domain center shown

Passing in open space – AMR and dynamic distribution

Domains of three-level refinement

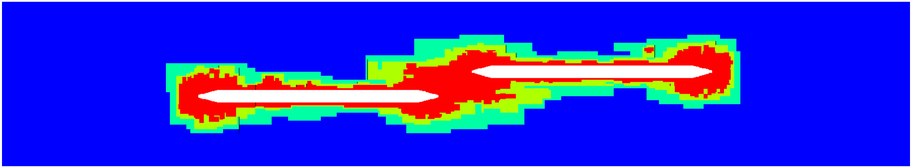

Distribution to 96 processors

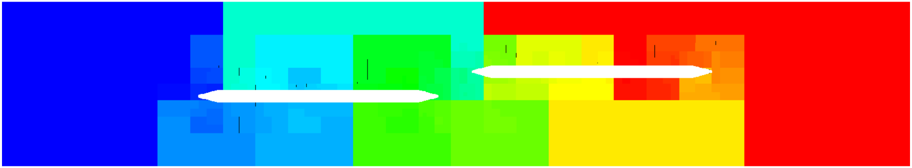

Enlargement of domain center shown

Passing in open space – AMR and dynamic distribution

Domains of three-level refinement

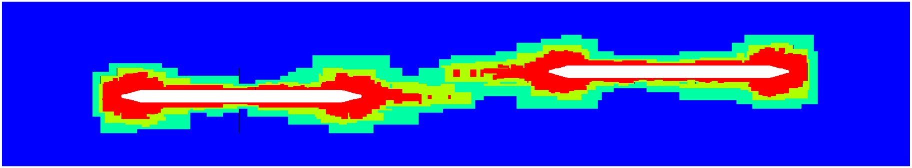

Distribution to 96 processors

Enlargement of domain center shown

Pressure isosurfaces

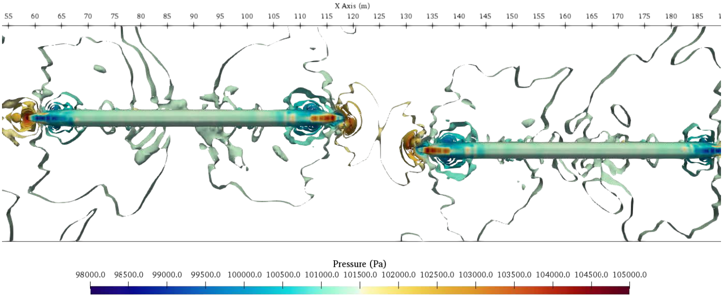

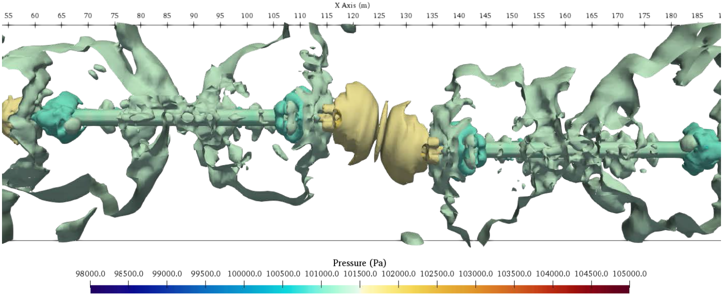

Pressure isosurfaces

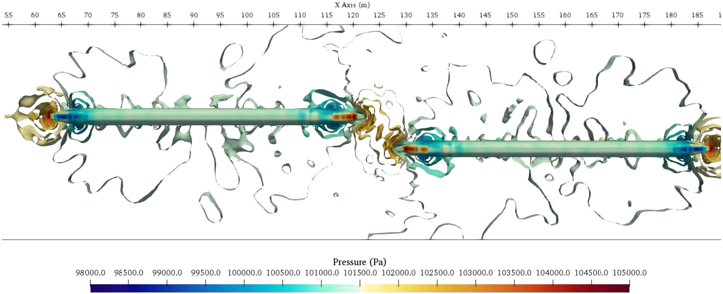

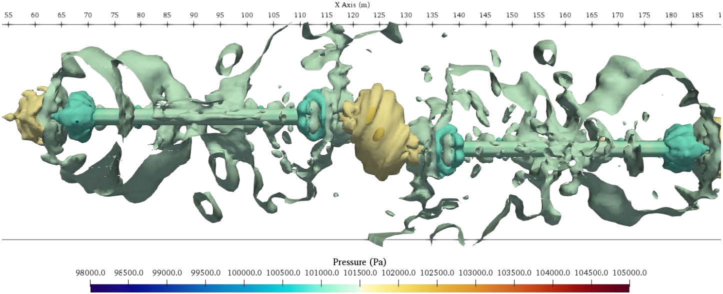

Pressure isosurfaces

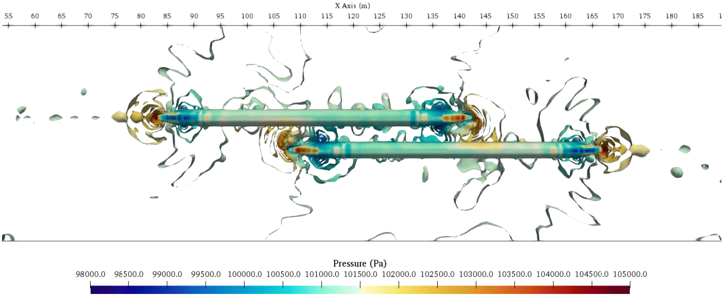

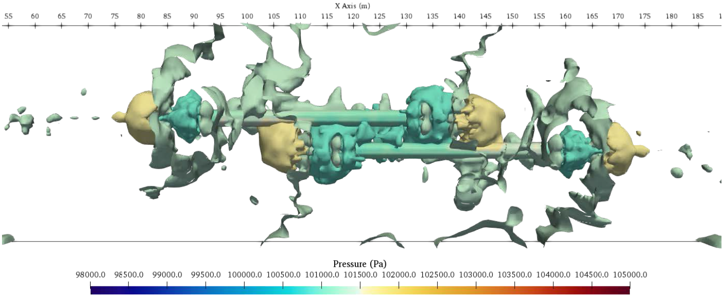

Pressure isosurfaces

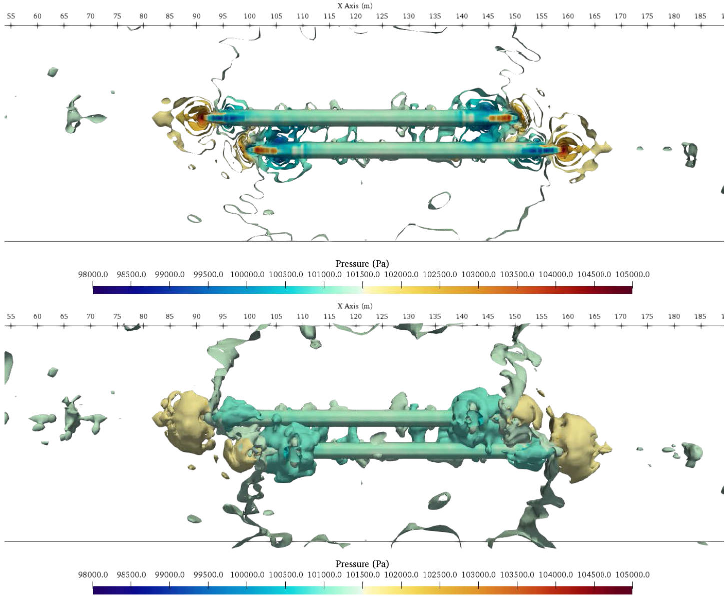

Pressure isosurfaces

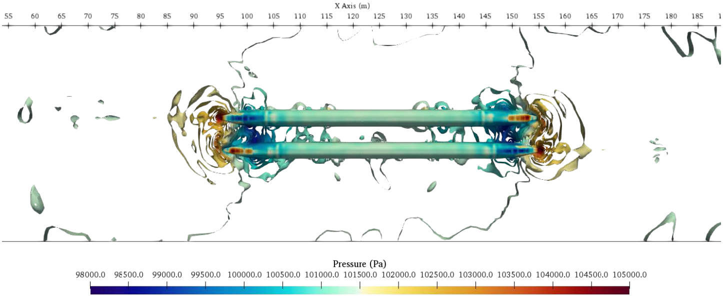

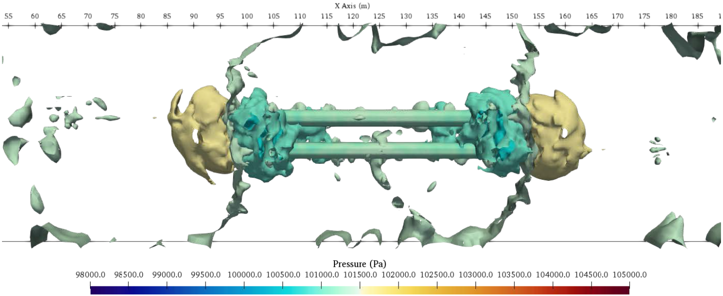

Pressure isosurfaces

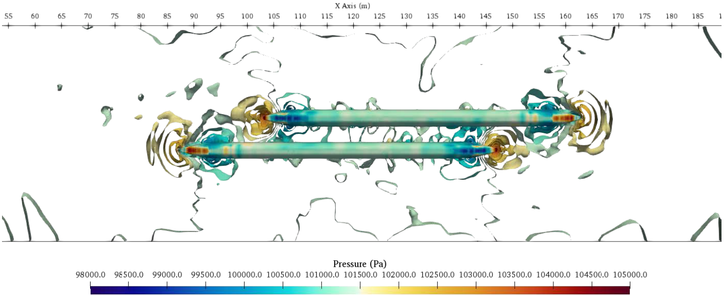

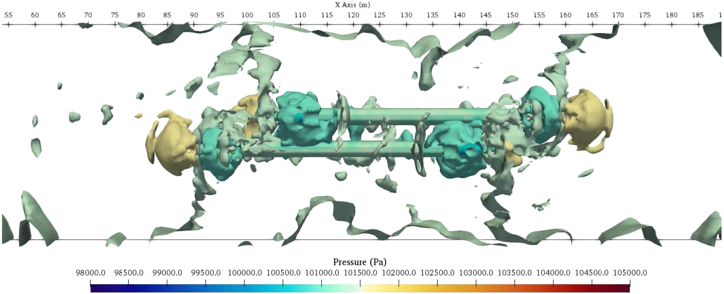

Pressure isosurfaces

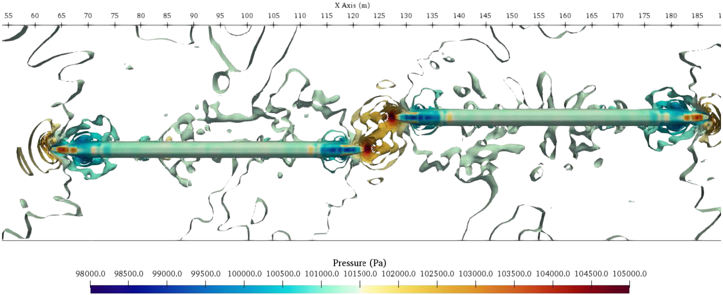

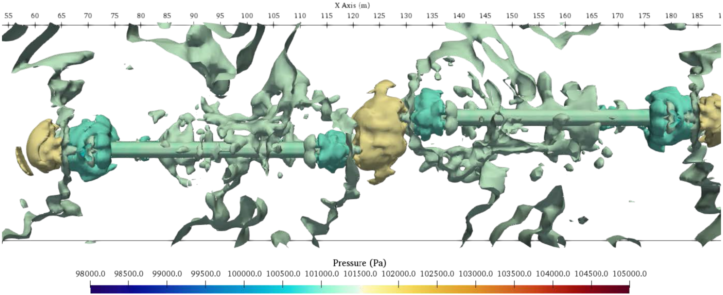

Pressure isosurfaces

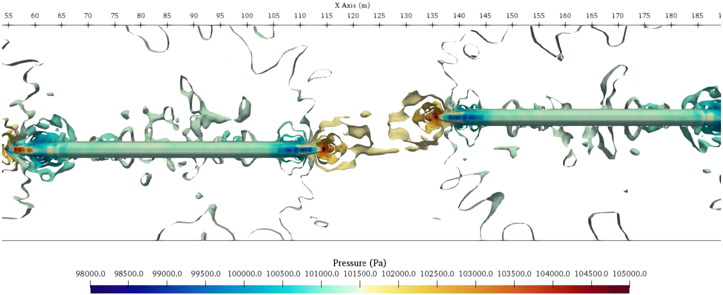

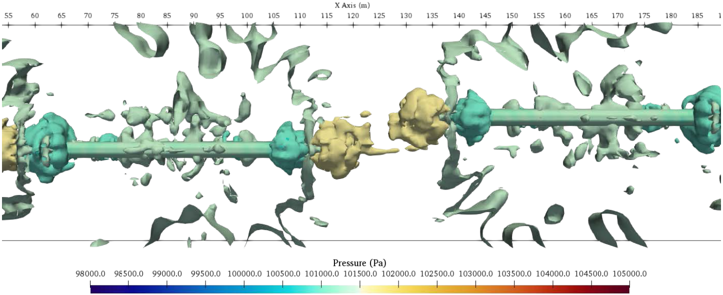

Pressure transects

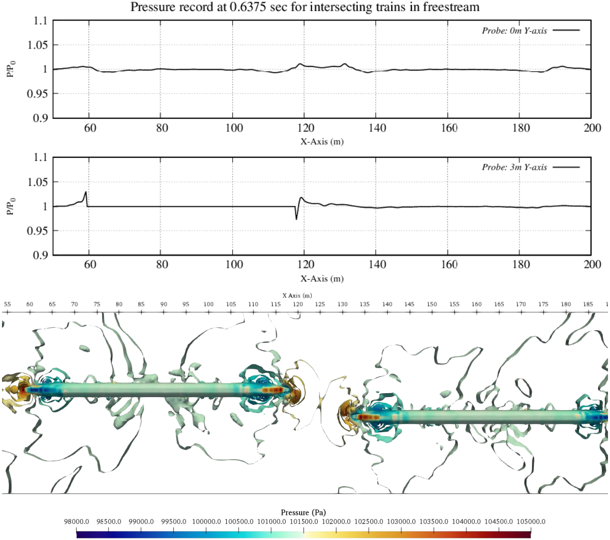

Pressure transects

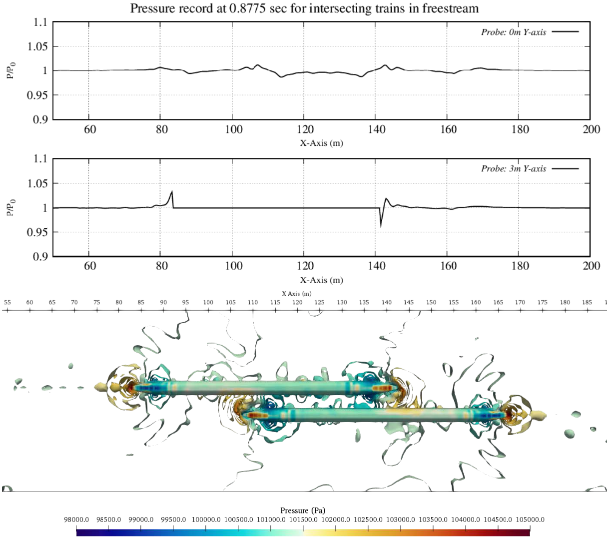

Pressure transects

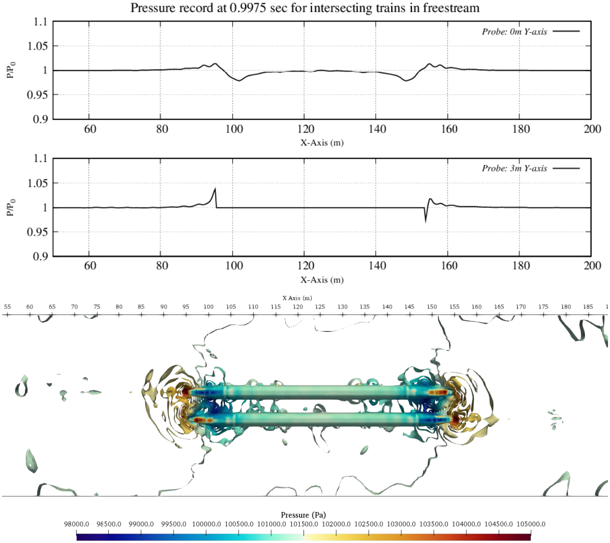

Pressure transects

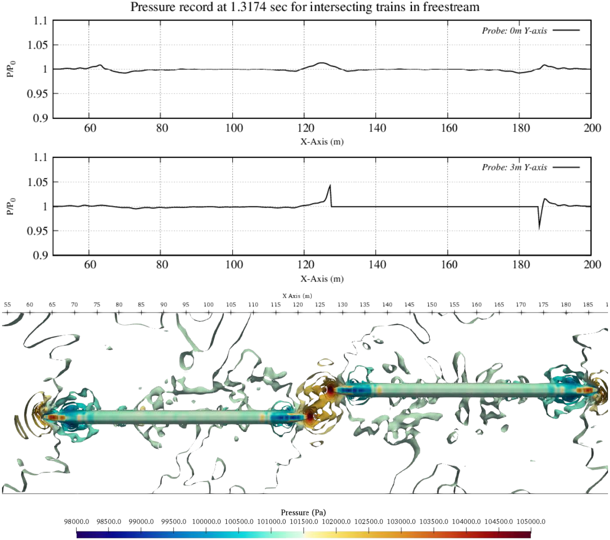

Setup with realistic tunnel shape

- Two NGT2 trains again at velocities $100\,\mathrm{m/s}$ and $-100\,\mathrm{m/s}$
- Prototype straight double track tunnel of $640\,\mathrm{m}$ length, initial distance between centers of trains $820\,\mathrm{m}$
- Base mesh of $1060 \times 36 \times 24$ for domain of $1060\,\mathrm{m} \times 36\,\mathrm{m} \times 24\,\mathrm{m}$, three levels refined by $r_{1,2,3} = 2$
- On 96 cores Intel Xeon E5-2670 $2.6\,\mathrm{GHz}$ a final $t_e = 5\,\mathrm{sec}$ was reached after $84,651\,\mathrm{sec}$ wall time, i.e., $2257\,\mathrm{h}$ CPU

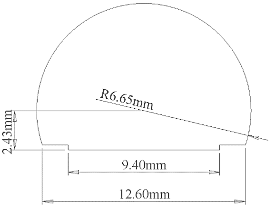

Tunnel shape

Setup with realistic tunnel shape

- Two NGT2 trains again at velocities $100\,\mathrm{m/s}$ and $-100\,\mathrm{m/s}$
- Prototype straight double track tunnel of $640\,\mathrm{m}$ length, initial distance between centers of trains $820\,\mathrm{m}$
- Base mesh of $1060 \times 36 \times 24$ for domain of $1060\,\mathrm{m} \times 36\,\mathrm{m} \times 24\,\mathrm{m}$, three levels refined by $r_{1,2,3} = 2$
- On 96 cores Intel Xeon E5-2670 $2.6\,\mathrm{GHz}$ a final $t_e = 5\,\mathrm{sec}$ was reached after $84,651\,\mathrm{sec}$ wall time, i.e., $2257\,\mathrm{h}$ CPU

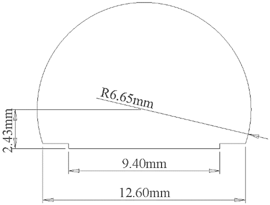

Tunnel shape

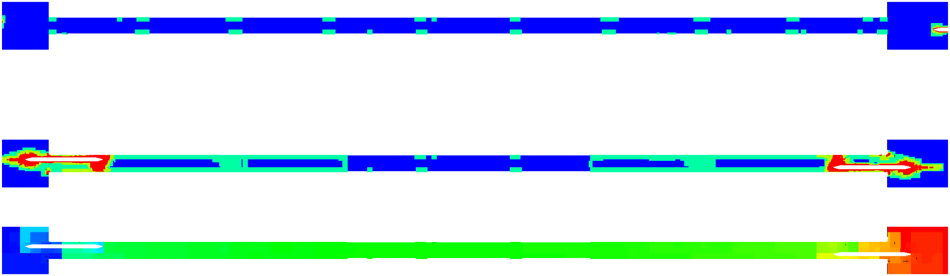

Setup with realistic tunnel shape

- Two NGT2 trains again at velocities $100\,\mathrm{m/s}$ and $-100\,\mathrm{m/s}$
- Prototype straight double track tunnel of $640\,\mathrm{m}$ length, initial distance between centers of trains $820\,\mathrm{m}$
- Base mesh of $1060 \times 36 \times 24$ for domain of $1060\,\mathrm{m} \times 36\,\mathrm{m} \times 24\,\mathrm{m}$, three levels refined by $r_{1,2,3} = 2$
- On 96 cores Intel Xeon E5-2670 $2.6\,\mathrm{GHz}$ a final $t_e = 5\,\mathrm{sec}$ was reached after $84,651\,\mathrm{sec}$ wall time, i.e., $2257\,\mathrm{h}$ CPU

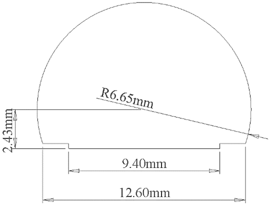

Tunnel shape

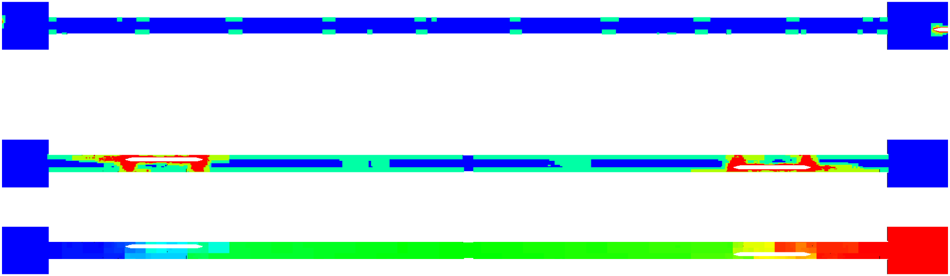

Setup with realistic tunnel shape

- Two NGT2 trains again at velocities $100\,\mathrm{m/s}$ and $-100\,\mathrm{m/s}$
- Prototype straight double track tunnel of $640\,\mathrm{m}$ length, initial distance between centers of trains $820\,\mathrm{m}$
- Base mesh of $1060 \times 36 \times 24$ for domain of $1060\,\mathrm{m} \times 36\,\mathrm{m} \times 24\,\mathrm{m}$, three levels refined by $r_{1,2,3} = 2$
- On 96 cores Intel Xeon E5-2670 $2.6\,\mathrm{GHz}$ a final $t_e = 5\,\mathrm{sec}$ was reached after $84,651\,\mathrm{sec}$ wall time, i.e., $2257\,\mathrm{h}$ CPU

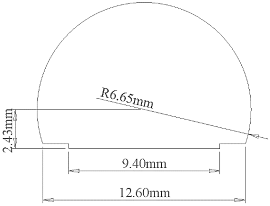

Tunnel shape

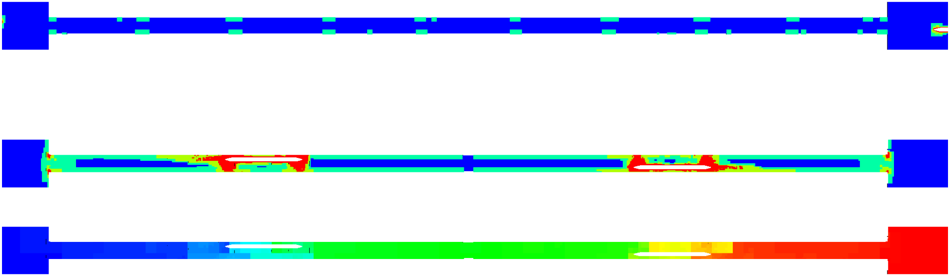

Setup with realistic tunnel shape

- Two NGT2 trains again at velocities $100\,\mathrm{m/s}$ and $-100\,\mathrm{m/s}$
- Prototype straight double track tunnel of $640\,\mathrm{m}$ length, initial distance between centers of trains $820\,\mathrm{m}$
- Base mesh of $1060 \times 36 \times 24$ for domain of $1060\,\mathrm{m} \times 36\,\mathrm{m} \times 24\,\mathrm{m}$, three levels refined by $r_{1,2,3} = 2$
- On 96 cores Intel Xeon E5-2670 $2.6\,\mathrm{GHz}$ a final $t_e = 5\,\mathrm{sec}$ was reached after $84,651\,\mathrm{sec}$ wall time, i.e., $2257\,\mathrm{h}$ CPU

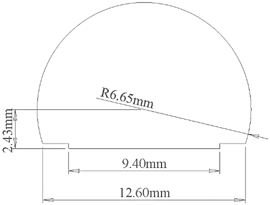

Tunnel shape

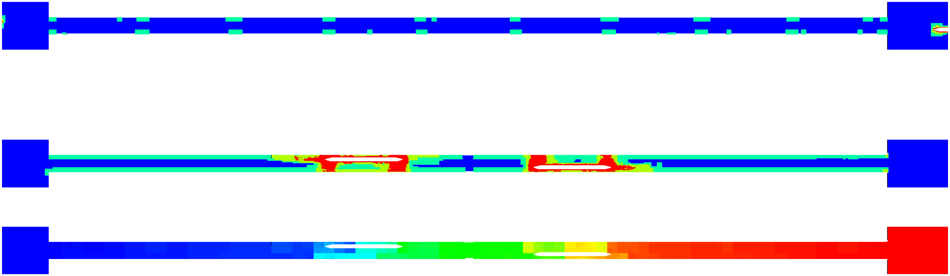

Setup with realistic tunnel shape

- Two NGT2 trains again at velocities 100 $\mathrm{m/s}$ and $-100\,\mathrm{m/s}$
- Prototype straight double track tunnel of 640 m length, initial distance between centers of trains 820 m
- Base mesh of $1060 \times 36 \times 24$ for domain of $1060\,\mathrm{m} \times 36\,\mathrm{m} \times 24\,\mathrm{m}$, three levels refined by $r_{1,2,3} = 2$
- On 96 cores Intel Xeon E5-2670 2.6 GHz a final $t_e = 5\,\mathrm{sec}$ was reached after 84,651 sec wall time, i.e., 2257 h CPU

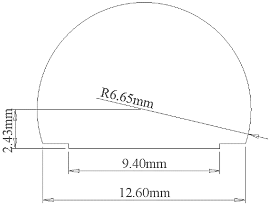

Tunnel shape

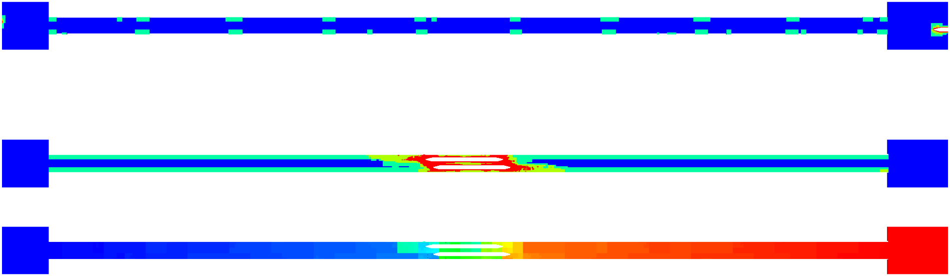

Setup with realistic tunnel shape

- Two NGT2 trains again at velocities $100\,\mathrm{m/s}$ and $-100\,\mathrm{m/s}$
- Prototype straight double track tunnel of $640\,\mathrm{m}$ length, initial distance between centers of trains $820\,\mathrm{m}$
- Base mesh of $1060 \times 36 \times 24$ for domain of $1060\,\mathrm{m} \times 36\,\mathrm{m} \times 24\,\mathrm{m}$, three levels refined by $r_{1,2,3} = 2$
- On 96 cores Intel Xeon E5-2670 $2.6\,\mathrm{GHz}$ a final $t_e = 5\,\mathrm{sec}$ was reached after $84,651\,\mathrm{sec}$ wall time, i.e., $2257\,\mathrm{h}$ CPU

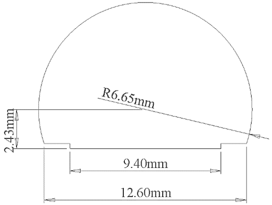

Tunnel shape

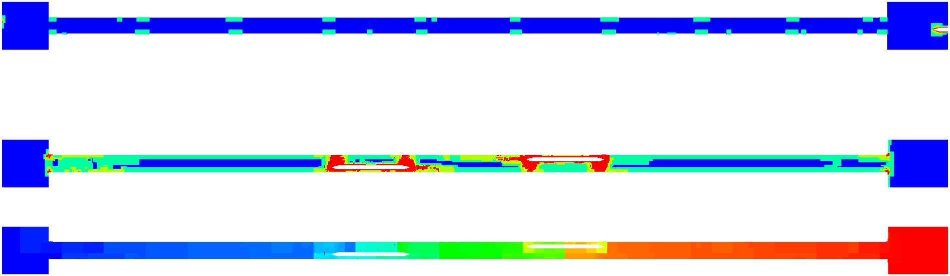

Pressure transects

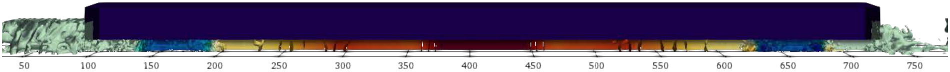

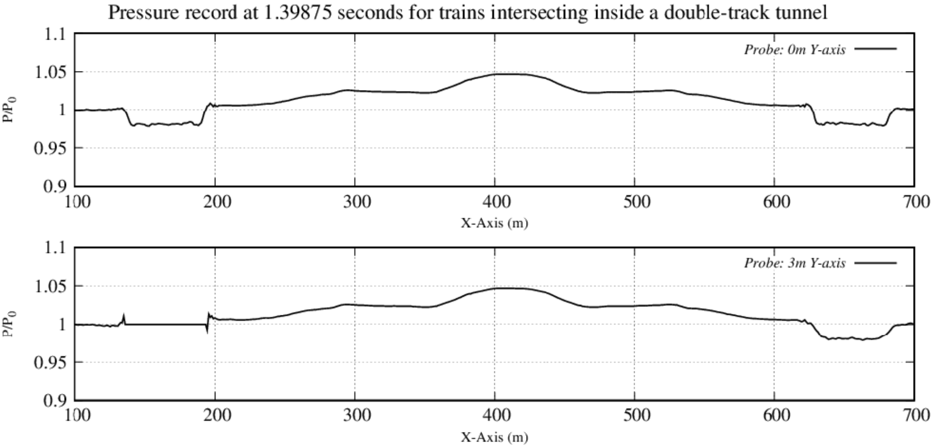

Pressure transects

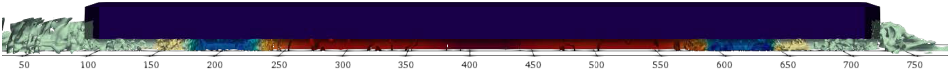

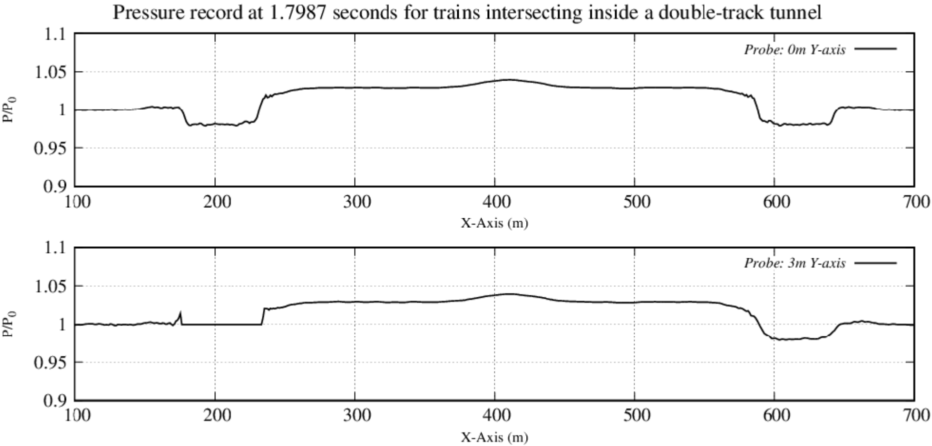

Pressure transects

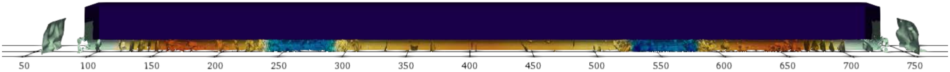

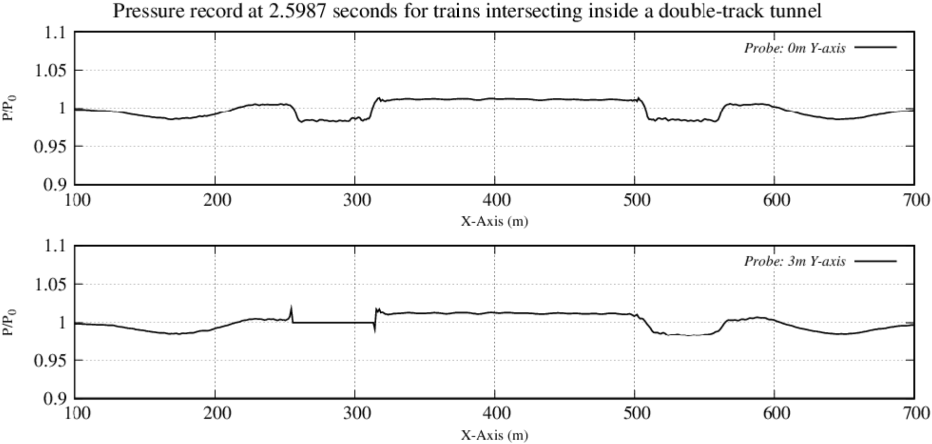

Pressure transects

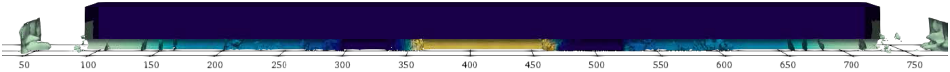

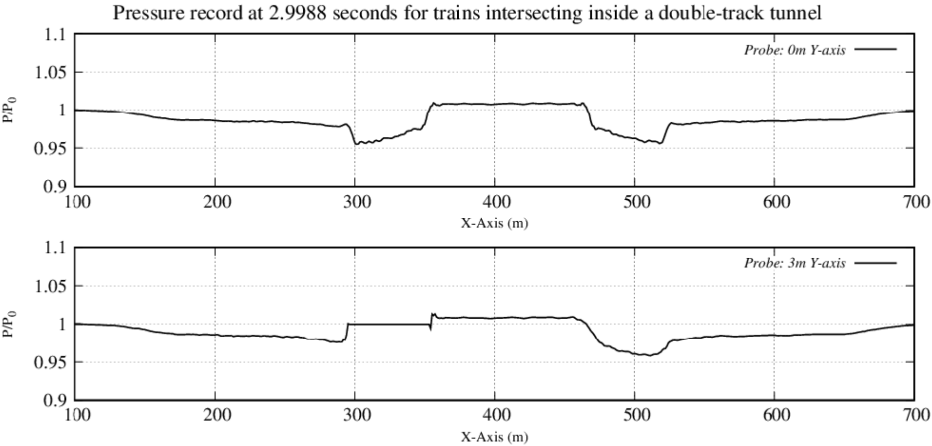

Pressure transects

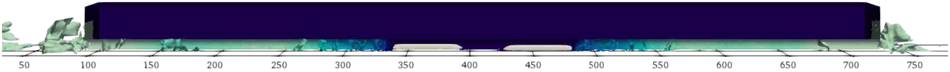

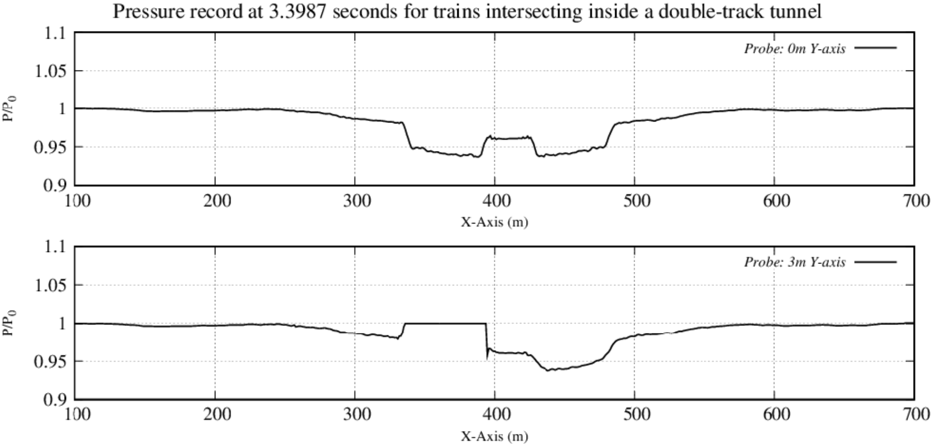

Conclusions – compressible flow aerodynamics

- A Cartesian embedded boundary method for compressible flows with block-based adaptive mesh refinement is an efficient and scalable prediction tool for pressure and shock waves created by moving bodies

Conclusions – compressible flow aerodynamics

- A Cartesian embedded boundary method for compressible flows with block-based adaptive mesh refinement is an efficient and scalable prediction tool for pressure and shock waves created by moving bodies
- Multi-resolution and fluid-structure coupling problems can be tackled without expensive mesh regeneration
  - Level set approach easily handles large motions, element failure and removal
  - Dynamic adaptation ensures high resolution at embedded boundaries and essential flow features

Conclusions – compressible flow aerodynamics

- A Cartesian embedded boundary method for compressible flows with block-based adaptive mesh refinement is an efficient and scalable prediction tool for pressure and shock waves created by moving bodies
- Multi-resolution and fluid-structure coupling problems can be tackled without expensive mesh regeneration
  - Level set approach easily handles large motions, element failure and removal
  - Dynamic adaptation ensures high resolution at embedded boundaries and essential flow features
- Aerodynamics of bodies with large motion are easily accessible
  - Current inviscid approach predicts maximal overpressure in front of trains reliably
  - For predicting the flow around entire trains, the boundary layer growing over the train body needs to be considered.
  - AMROC solvers for the compressible Navier-Stokes equations and even LES are already available, however, for this particular application a turbulent wall function on the embedded boundary first needs to be implemented. Such a wall function is currently work-in-progress for the LBM-LES solver.

References I

[Arienti et al., 2003] Arienti, M., Hung, P., Morano, E., and Shepherd, J. E. (2003). A level set approach to Eulerian-Lagrangian coupling. *J. Comput. Phys.*, 185:213–251.

[Cirak et al., 2007] Cirak, F., Deiterding, R., and Mauch, S. P. (2007). Large-scale fluid-structure interaction simulation of viscoplastic and fracturing thin shells subjected to shocks and detonations. *Computers & Structures*, 85(11-14):1049–1065.

[Deiterding et al., 2006] Deiterding, R., Radovitzky, R., Mauch, S. P., Noels, L., Cummings, J. C., and Meiron, D. I. (2006). A virtual test facility for the efficient simulation of solid materials under high energy shock-wave loading. *Engineering with Computers*, 22(3-4):325–347.

[Deiterding and Wood, 2013] Deiterding, R. and Wood, S. L. (2013). Parallel adaptive fluid-structure interaction simulations of explosions impacting on building structures. *Computers & Fluids*, 88:719–729.

[Fedkiw, 2002] Fedkiw, R. P. (2002). Coupling an Eulerian fluid calculation to a Lagrangian solid calculation with the ghost fluid method. *J. Comput. Phys.*, 175:200–224.

[Fragner and Deiterding, 2016] Fragner, M. M. and Deiterding, R. (2016). Investigating cross-wind stability of high speed trains with large-scale parallel cfd. *Int. J. Comput. Fluid Dynamics*, 30:402–407.

[Fragner and Deiterding, 2017] Fragner, M. M. and Deiterding, R. (2017). Investigating side-wind stability of high speed trains using high resolution large eddy simulations and hybrid models. In Diez, P., Neittaanmäki, P., Periaux, J., Tuovinen, T., and Bräysy, O., editors, *Computational Methods in Applied Sciences*, volume 45, pages 223–241. Springer.

[Giordano et al., 2005] Giordano, J., Jourdan, G., Burtschell, Y., Medale, M., Zeitoun, D. E., and Houas, L. (2005). Shock wave impacts on deforming panel, an application of fluid-structure interaction. *Shock Waves*, 14(1-2):103–110.

[Laurence and Deiterding, 2011] Laurence, S. J. and Deiterding, R. (2011). Shock-wave surfing. *J. Fluid Mech.*, 676:369–431.

[Laurence et al., 2007] Laurence, S. J., Deiterding, R., and Hornung, H. G. (2007). Proximal bodies in hypersonic flows. *J. Fluid Mech.*, 590:209–237.

[Luccioni et al., 2004] Luccioni, B. M., Ambrosini, R. D., and Danesi, R. F. (2004). Analysis of building collapse under blast loads. *Engineering & Structures*, 26:63–71.

[Mader, 1979] Mader, C. L. (1979). *Numerical modeling of detonations*. University of California Press, Berkeley and Los Angeles, California.

References II

[Mauch, 2003] Mauch, S. P. (2003). *Efficient Algorithms for Solving Static Hamilton-Jacobi Equations*. PhD thesis, California Institute of Technology.

[Sethian, 1999] Sethian, J. A. (1999). *Level set methods and fast marching methods*. Cambridge University Press, Cambridge, New York.

[Specht, 2000] Specht, U. (2000). *Numerische Simulation mechanischer Wellen an Fluid-Festkörper-Mediengrenzen*. Number 398 in VDI Reihe 7. VDU Verlag, Düsseldorf.

[Zonglin et al., 2002] Zonglin, J., Matsuoka, K., Sasoh, A., and Takayama, K. (2002). Numerical and experimental investigation of wave dynamics processes in high-speed train/tunnels. *Chinese Journal of Mechanics Press*, 18(3):210–226.